The Hong Kong Polytechnic University

The Interdisciplinary Division of Biomedical Engineering

CHARACTERIZATION OF THE COLORECTAL CANCER

BY

COMBINING HIGH-FREQUENCY ENDOSCOPIC ULTRASOUND

AND

QUANTITATIVE ULTRASOUND

Cheng LIU

A thesis submitted in partial fulfillment of the requirements for

the degree of Master of Philosophy

July 2013

CERTIFICATE OF ORIGINALITY

I hereby declare that this thesis is my own work and that, to the best of my knowledge and belief, it reproduces no material previously published or written, nor material that has been accepted for the award of any other degree of diploma, except where due acknowledgement has been made in the text.

Cheng LIU

July 2013

DEDICATION

This thesis is dedicated to my family

ABSTRACT

Colorectal cancer (CRC) is the third most common cancer for both men and women in the US, predicted in 2012 to account for 9% of new cases and cancer related deaths. The fact that only 39% of pre-cancerous colorectal tumors are detected at an early stage is the main factor that leads to metastasis and high mortality rate. The invasion depth of early CRC limits to superficial layers of colorectal wall with few vascular and lymphatic vessels. CRC at early stage often has no symptoms, which causes delay of successful treatments. Colonoscopy is clinically performed for screening, during which biopsy may be conducted; however, it is difficult to determine early stage CRC by ordinary endoscopy even with dye due to the insufficient superficial scope of colorectal surface for pre-cancerous diagnosis.

Endoscopic ultrasound (EUS) has been widely used to visualize overall depth-view five-layered structural alteration of colorectal tract. With high-frequency transducer (20MHz-30MHz), EUS is capable of delineating the mucosa-submucosa layer of normal human colon with micron-scale resolution anatomical information; however, the current high-frequency EUS is still insufficient to distinguish cancer from polyp and adenoma due to the lack of patho-physiological information. An open high-frequency EUS system, compatible with regular endoscope, which allows acquisition of radio frequency (RF) data for acoustic tissue characterization and combination with other functional imaging modalities (e.g. photoacoustic imaging) may bring values to diagnose colorectal malignancies.

The development of a novel high-frequency EUS system which allows quantitative acoustic tissue characterization and easy fusion of multiple functional modalities for complementary structural & patho-physiological information is presented in this chapter. Processed B-mode images or unprocessed raw RF data could be stored, displayed and post-processed in PC. A miniaturized 30.5 MHz single element mechanical side-view EUS transducer was fabricated using PMN-0.28PT single crystal. Phantom test, *ex vivo* imaging of swine, mouse and rabbit colon specimen, and *in vivo* imaging of rabbit were conducted to evaluate the performance of the system. New Zealand White male rabbits surgically implanted with VX2 tumor cell were used for characterization of CRC tissue and normal colon tissue. *Ex vivo* scan was performed to acquire B-mode images and raw RF data. The acoustic spectra analysis was performed. Intercept, slope and midband fit were obtained and compared between the region-of interests (ROIs) representing colorectal tumors and normal colon tissue. The results of ex vivo B-mode image, color-coded image were compared with histology.

Testing results showed that the system could detect a minimum signal of 25 μV, allowing a 50 dB dynamic range at 45 dB gain, with a frequency range from 20 MHz to 100 MHz. Finally, phantom imaging, in vivo imaging of normal colon in ICR mouse and New Zealand White rabbit model were conducted to demonstrate the performance of the system. Significant differences were observed between the parameters from cancerous ROIs and normal tissue region. The results showed that the complementary

information derived from quantitative high-frequency EUS may create better sensitivity and specificity to colorectal cancer diagnosis.

PUBLICATIONS ARISING FROM THE THESIS

Peer-reviewed Journal Paper

W. Qiu, Y. Yu, H. R. Chabok, **C. Liu**, F. K. Tsang, Q. Zhou, K. K. Shung, H. Zheng, L. Sun, A flexible annular array imaging platform for micro-ultrasound, IEEE Transactions on Ultrasonics Ferroelectrics and Frequency Control, vol. 60, no. 1, pp. 178-186, 2013.

Conference Proceedings

1. Cheng LIU, Weibao QIU, Yanyan YU, Lei SUN, Characterization of the Colorectal Cancer in a Rabbit Model Using Quantitative High-frequency Endoscopic Ultrasound, Proceedings, Joint UFFC, EFTF, and PFM Symposium, Prague, Czech Republic, pp. 891-894, 21-25 July 2013

2.Cheng LIU, Weibao QIU, Yan CHEN, Yanyan YU, Jiyan DAI, Lei SUN, A Novel High-frequency Endoscopic Ultrasound System for Colorectal Cancer Diagnosis, Proceedings, Joint UFFC, EFTF, and PFM Symposium, Prague, Czech Republic, pp. 2045-2048, 21-25 July 2013

3.Cheng LIU, Yan CHEN, Weibao QIU, Yanyan YU, Jiyan DAI, Lei SUN, A Novel High-frequency Endoscopic Ultrasound System for In Vivo Imaging of Colorectal Cancer in a Rabbit Model, Proceedings, The 6th WACBE World Congress on Bioengineering, Beijing, China, pp. 383, 5-8 August 2013

ACKNOWLEDGMENTS

I would like to express my sincere thanks to my chief supervisor, Assistant Professor Dr. Lei SUN for his continuous guidance, supervision, invaluable comments. Thanks for his patience, encouragement and the effort he made on me. I will be forever grateful everything he has done.

I would like to thank Associate Professor Dr. Mo Yang, Assistant Professor Dr. Thomas Ming-Hung Lee for assessing my proposal, confirmation report, providing valuable suggestions and pointing out problems existing in my work and presentations.

I would especially thank Associate Professor Dr. Jiyan DAI for the guidance and help in the transducer fabrication. I would thank my colleague Associate Professor Dr. Weibao QIU for his support and guidance in experimental system setup. Also thanks to Dr. Shaowei ZHENG, Dr. Guixiang YANG for their sincere help in the animal experiments. Many thanks to Dr. Yan CHEN, Mrs Yanyan YU, Mr. Fu Keung Tsang Tommy, Mr. Han XU, Mr. Yaoheng YANG, Miss Weiwei YE for their selfless support. These lovely colleagues made this a wonderful experience.

To all the subjects who were involved in this project, I would like to thank for their time to my study. Without their active participation, this study would not be possible. Last but not least, I would like to give my heartfelt thanks to my dearest families for their tender love and for understanding of what I have been pursuing all these years.

TABLE OF CONTENTS

LIST OF ABBREVIATIONS

3D	Three-dimensional
ADC	Analog-to-digital converter
BPF	Band pass filter
CRC	Colorectal Cancer
CT	Computed tomography
DAC	Digital-to-analog converter
DSP	Digital signal processing
DOF	Depth of field
EUS	Endoscopic ultrasound
FFT	Fast fourier transform
FPGA	Field programmable gate array
GUI	Graphical user interface
H&E	Hematoxylin and eosin stain
$LiNbO_3$	Lithium niobate
MHz	Mega-hertz
MSPS	Mega-samples per second
MRI	Magnetic resonance imaging
PCB	Printed circuit board
PCIE	Peripheral component interconnect express
PMN-PT	Lead magnesium niobate-lead titanate
PW	Pulsed-wave
QUS	Quantitative ultrasound
RF	Radio frequency
ROI	Region of interest
SNR	Signal-to-noise ratio
SPSS	Statistical package for social science
TGC	Time gain compensation
USB	Universal serial bus

CHAPTER 1 INTRODUCTION

1.1 RESEARCH BACKGROUND

Colorectal cancer (CRC) is the third most common cancer for both men and women in the United States, predicted in 2012 to account for 9% of newly diagnosed malignancies and 9% of cancer related deaths. There are about 150,000 new cases per year in the United States which affects 5% of population. There were also 51,290 deaths caused by CRC in the United States in 2012 alone which ranks the 2nd in cancer related mortality (Atlanta: American Cancer Society 2011). CRC typically begins as benign polyps of which up to 50% may develop to cancerous malignancies if left untreated for a long period of 10 to 15 years (Siegel et al. 2013). Early stage CRC and polyps often cause no obvious symptoms and result in delay of timely and successful treatments. The fact that only 39% of pre-cancerous colorectal tumors are detected at an early, localized stage is the main factor that leads to cancer metastasis and high mortality rate (Siegel et al. 2013). However, CRC is one of the most potentially preventable and curable gastrointestinal cancers at early stage (Anderson 2011). These characteristics render CRC a significant disease for early diagnosis, both for detection of cancer at treatable stages before metastasis, and more importantly, detection and removal of high-risky pre-cancerous abnormalities.

In clinical, tumor is largely assessed based on the evidence of morphological changes. 90% of localized malignant colorectal tumors at early stages could be cured (Atlanta:

American Cancer Society 2011). Obvious morphological changes may not occur at all for colorectal tumors at early stage. Recently, treatment for colorectal cancer has become increasingly differentiated. Patients with early stage colorectal neoplasia limited to the mucosal layer can be cured with endoscopic treatment [ref]. In those with more advanced stages, surgical treatment should be considered. The most popular diagnostic tool for the detection of lesions in colorectal tract, such as polyps, neoplasia and malignant tumor is colonoscopy although it could only visualize the surface of colorectal tract (Atlanta: American Cancer Society 2011). Benign lesions, such as polyps could effectively be cured by endoscopic resection. In contrast, differentiation of malignant tumors which are possible to metastasize to adjacent organs requires patho-physiological information and penetration depth information for accurate lesion staging and treatment strategy. Therefore, complementary information acquired with routine colonoscopy which is able to determine the tissue's patho-physiology and penetration depth through colorectal wall would bring great potential for accurate early detection of colorectal cancer.

Surgery to remove the colorectal tumors is often the main treatment except for those patients with distant metastatic malignancies. Adjuvant therapy, such as chemotherapy and radiation, are often used as additional treatment strategy to surgery on the purpose of reducing the risk of recurrence and metastasis. As an indispensable section of the treatment strategy in clinical, postoperative surveillance assesses the efficacy of initial therapy routinely, more importantly, periodic exams for treated patients may lead to earlier identification and management of recurrent disease. A statistically significant 5-year survival benefit has been demonstrated for more intensive follow-up protocols in

clinical trials (Pietra et al 1998; Secco et al 2002; Huang et al 2007). This also demands a sensitive and accurate method to facilitate postoperative surveillance to identify recurrence during periodic examination.

1.2 RESEARCH SIGNIFICANCE

Early colorectal cancers (CRC) show diversity in configuration. It is difficult to distinguish cancer from adenoma and hyperplastic polyp by ordinary endoscope observation even with dye. The magnifying endoscope has improved the diagnosis accuracy on the degree of lesion invasion. Oral intake capsule endoscope has been reported to be useful for detection of small lesions. Recently, color-enhanced electronic endoscope has become popular due to its ability to show superficial capillary blood vessel (Anderson 2011). Since the ability to recognize the five-layered structure of the gastrointestinal tract, endoscopic ultrasound (EUS) has been widely used to visualize overall structures of gastrointestinal tract for determining the local surgery strategy (Pietra et al 1998). However, its potential to diagnose early colorectal cancers has not been noticed until the appearance of mini high frequency transducer and high frequency ultrasound instrument.

High-frequency EUS is capable of high-resolution delineation of the colorectal tract; however, itself alone is not sensitive and specific enough to the tumor cells microstructural and pathological conditions change. Accurate CRC diagnosis and staging need to characterize the lesions pathology, in addition to identify morphological alteration. Emerging and existing technologies that can obtain functional/physiological

characteristics, e.g. ultrasonic tissue characterization (Kumon et al. 2012), photoacoustic imaging (PAI) (Yang et al. 2012), optical tomography (Zhu et al. 2010) have the potentials in early stage colorectal diseases diagnosis. Combining these techniques to form a dual- or multi- modality imaging may supplement the strength of individual technology and achieve a comprehensive and precise CRC diagnosis.

Since the ability to recognize the five-layered structure of colorectal wall and adjacent organs beyond surface, conventional low-frequency (7.5MHz-12MHz) endoscopic ultrasound (EUS) has been used as the standard clinical tool for years along with other modalities for colorectal cancer staging to assess tumor penetration and evaluate metastasis possibilities (Lightdale and Kulkarni 2005). More importantly, EUS could provide real time, high-resolution, cross-sectional side-view imaging over a large field of view (FOV) at low frequency (Yang et al. 2012). Compared with other medical imaging modalities, such as magnetic resonance imaging (MRI), X-ray computed tomography (X-ray CT) and positron emission tomography (PET), EUS transducer is embodied in an endoscopic tube, uses safe mechanical waves and permits routine bedside exams. Recent studies have shown that at higher frequency (>20MHz), EUS is capable of delineating the mucosa-submucosa layer of normal human colorectal tract with fine resolution anatomical information which allows more precise visualization and staging of colorectal cancer (Haji et al. 2012,Hurlstone et al. 2005).

Although EUS imaging has shown its ability for various applications, most of the current applications of EUS are focused to guide other interventional operations based on its high-resolution overall structure image. Early-stage cancer detection or *in situ*

characterization of abnormal tissues is challenging for EUS because its image contrast mechanism relies on bulk mechanical properties. Conventional B-mode EUS images can be constructed by displaying only the amplitude of the envelope of the underlying radiofrequency (RF) ultrasound signals received by a broad bandwidth ultrasound transducer as image brightness. However, images generated this way are subjected to the loss of tissue information derived from raw RF data and a variety of factors including the electronic ultrasound (US) system response, ultrasound transducer response and image post-processing, rendering the results operator- and system dependent. Hence, to generate images that represent objective tissue properties and permit easy comparison of images obtained with different settings or systems, methods need to be developed to remove or minimize these factors.

Quantitative ultrasound (QUS) is a promising technique for non-invasive tissue characterization. The field of knowledge of high-frequency EUS with QUS for colorectal cancer diagnosis is yet to be fully determined and a reproducible and feasible animal model is appropriate for further development of this novel modality. VX2 CRC Rabbit model is first time used as a model for endoscopic ultrasound imaging according to our knowledge. In this work, the potential to assess QUS in colorectal cancer tissue was examined. Specifically, the QUS parameters were evaluated in respect to their ability to discriminate between normal and cancerous colon tissue.

1.3 RESEARCH OBJECTIVES

In this study, I for the first time show the application of high-frequency endoscopic ultrasound (EUS) along with quantitative ultrasound (QUS) to characterize malignant colorectal tumor and benign colorectal tissue in a rabbit model of VX2 colorectal cancer. I have developed a novel high-frequency endoscopic ultrasound (EUS) system for real-time EUS and QUS imaging of colorectal cancer in preliminary studies. In this study our purpose was to validate RF spectral analysis as a method to distinguish between colorectal cancer (CRC) and benign colorectal wall.

The long-term objective of the colorectal cancer studies is to develop high-frequency endoscopic ultrasound imaging methods that are capable of detecting early stage colorectal cancer using complementary structural and functional information. This method would direct the endoscopist to suspicious regions that might be overlooked in routine EUS and endoscopy procedures. To achieve this objective, studies of quantitative high-frequency endoscopic ultrasound imaging methods that go beyond conventional, qualitative, B-mode imaging are being undertaken.

1.4 OUTLINE OF THE DISSERTATION

This dissertation is organized as follow:

After the present chapter, Chapter 2 outlines the background of the colorectal cancer in terms of its prevalence, colorectal anatomy, cancer staging, diagnostic methods and research gap.

In Chapter 3, the development of a novel high-frequency endoscopic ultrasound system is presented for the diagnosis of CRC followed by phantom and animal experiment evaluation results.

Chapter 4 discusses the quantitative ultrasound characterization of cancerous colon tissue and normal colon tissue in a rabbit model of colorectal cancer based on the novel high-frequency EUS system in Chapter 3.

Finally, Chapter 5 summarizes the findings and limitations of this study and suggests future work.

CHAPTER 2 LITERATURE REVIEW

2.1 PREVALENCE OF COLORECTAL CANCER

Colorectal malignancy is the third most common cancer for both men and women in the United States, predicted in 2012 to account for 9% of newly diagnosed malignancies and 9% of cancer related deaths (Atlanta: American Cancer Society 2011). The American Cancer Society recently estimated that there were 101,340 new cases of colon cancer, 39,870 new cases of rectal cancer and 49,380 deaths in 2011 alone (Atlanta: American Cancer Society 2011). Hong Kong studies show that colorectal malignancy increased most rapidly among other cancers since the late 1980s and accounted for more than 15% of all newly diagnostic malignancies and 13% of all cancer related deaths in the last five years (Hong Kong Cancer Registry, Hospital Authority, 2009). Early colorectal cancer often has no symptoms and results in delay of timely and successful treatments. Colorectal cancer typically begins as benign polyps of which 33% to 50% may develop to cancerous malignancies for a period of 10 to 15 years (Jemal et al 2010). The death rate of colorectal cancer (deaths number per 100,000 people per year) has been decreasing for both men and women for the past 20 years. One reason for the decreasing death rate is that screening is allowing more polyps and colorectal cancers to be found and cured at earlier stage. Another reason is that the treatment for colorectal cancer has been improving over the past years.

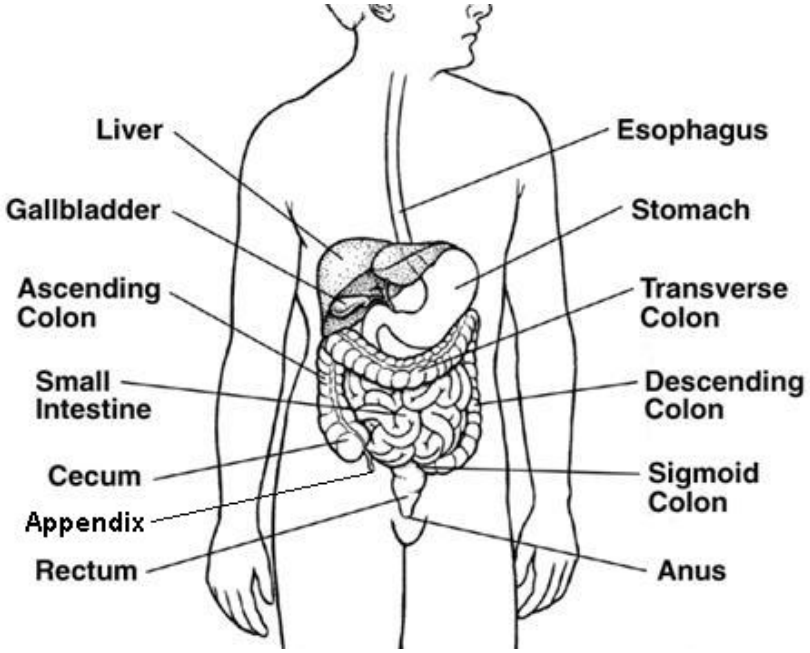

Figure 2.1.Diagram of Colon and Rectum (Atlanta: American Cancer Society 2011)

2.2 ANATOMY OF COLORECTAL TRACT

The colorectal wall is recognized as five-layered structure by EUS. From inside to outside, the wall is divided into mucosa (innermost layer), muscularis mucosa (thin inner muscle layer), submucosa (vascular and lymphatic layer), muscularis propria (thick outer muscle layer), subserosa and serosa (visceral peritoneum which covers most colon but not rectum). The invasion depth of early colorectal cancer limits to mucosa (almost no lymphatic vessel), muscularis mucosa (lymphatic vessels appear on superficial surface) and submucosa (vascular and lymphatic vessels appear). Based on the fact that the risk of lymph node metastasis increases in proportion to the lymph vessel amount, metastasis is theoretically possible to happen for invasion to muscularis mucosa layer (Atlanta: American Cancer Society 2011).

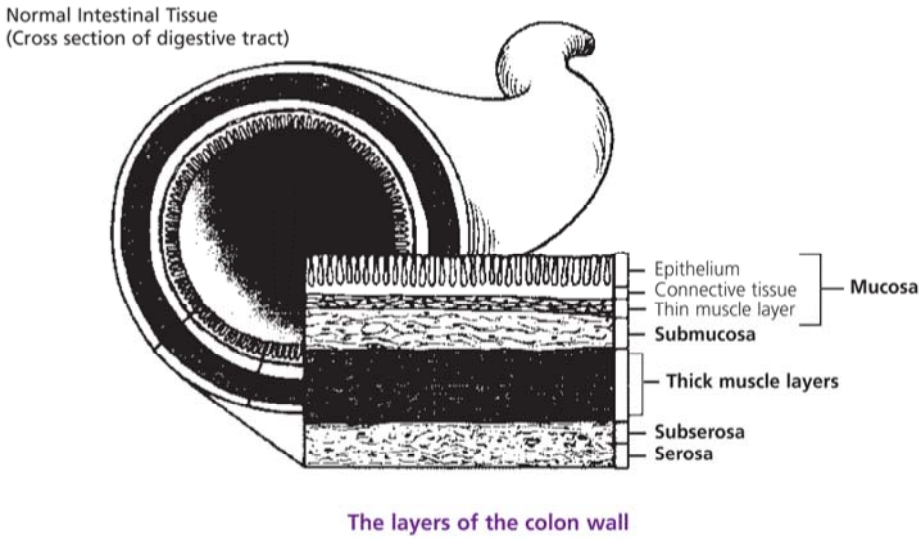

Figure 2.2.five-layered structure of colon (Atlanta: American Cancer Society 2011)

2.3 STAGING OF COLORECTAL CANCER

The TNM Classification of Malignant Tumors (TNM) is a cancer staging system that describes the extent of a person's cancer (Atlanta: American Cancer Society 2011).

- T describes the size of the original (primary) tumor and whether it has invaded nearby tissue,
- N describes nearby (regional) lymph nodes that are involved,
- M describes distant metastasis (spread of cancer from one part of the body to another).

Figure 2.3 shows the relationship of cancer penetration depth and corresponding cancer stage.

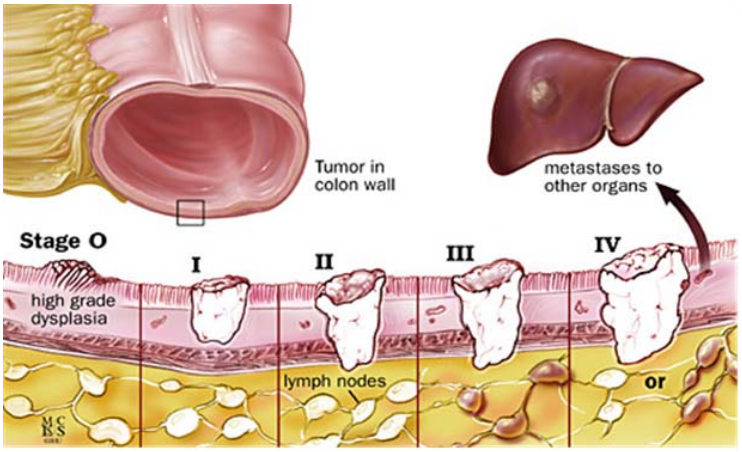

Figure 2.3.Colon cancer from T stage to M stage (Colorectal Cancer Center, Johns Hopkins Medicine) http://www.hopkinscoloncancercenter.org/JHH_Home.aspx?CurrentUDV=59）

Table 2.1.The TNM cancer staging system of colon cancer (Atlanta: American Cancer Society 2011)

T=primary tumor
TX=primary tumor cannot be assessed
T0=no evidence of primary tumor
Tis=carcinoma in situ: intraepithelial or invasion of lamina propria
T1=tumor invades submucosa
T2=tumor invades muscularis propria
T3=tumor invades through the muscularis propria into subserosa or into non-peritonealised pericolic or perirectal tissues
T4a=tumor penetrates the surface of the visceral peritoneum
T4b=tumor directly invades or is histologically adherent to other organs or structures
N=regional lymph nodes
NX=regional lymph nodes cannot be assessed
N0=no regional lymph node metastasis

N1a=metastasis in one regional lymph node
N1b=metastasis in two to three regional lymph nodes
N2a=metastasis in four to six regional lymph nodes
N2b=metastasis in seven or more regional lymph nodes
M=distant metastasis
MX=distant metastasis cannot be assessed
M0=no distant metastasis
M1a=distant metastasis to one site M1b=distant metastasis to more than one site

2.4 DIAGNOSIS OF COLORECTAL CANCER

Recommended colorectal cancer screening tests are divided into two groups:

1. Tests that can detect cancer and advanced lesions, which include flexible sigmoidoscopy, colonoscopy, barium enema, and Computed Tomography Colonography (CTC), Magnetic Resonance Imaging (MRI), Endoscopic Ultrasound (EUS)
2. Tests that primarily detect cancer, which include guaiac-based fecal occult blood testing (FOBT) and testing stool for exfoliated DNA (sDNA)

2.4.1 Flexible Sigmoidoscopy

Flexible sigmoidoscopy, which uses a sigmoidoscope with lighted tube and a small video camera on the front end, allows the visualization of the lower one third of the colon and rectum where 60% of cancers and adenomas are located (David et al., 2010).

During the test, the doctor inserts the sigmoidoscope into the lower part of the colon through the rectum to detect and remove any abnormalities. Images of the inside colorectal tract are displayed on a monitor. Because the length of the sigmoidoscope is only 60 cm, the doctor could only see less than half of colon in this test. Before the test, the patient will have to take a bowel preparation to clean out the lower colon. The test usually takes 10 to 20 minutes. If a benign polyp is found during the test, the doctor may remove it. The polyp will be sent for histology. If a pre-cancerous polyp or malignancy is found during the test, the patient will be suggested to have a following colonoscopy to look for abnormalities in the rest of the colon. Although it could only provide the superficial view of the colon tract, it is regarded as a noninvasive, low risk screening method for colorectal cancer (CRC) and the sensitivity of this method has been reported to be 55–92% (Rockey et al., 2005).

2.4.2 Colonoscopy

Similar to flexible sigmoidoscopy, colonoscopy allows direct visual examination of the colon and rectum as shown in Figure 2.4. Compared with flexible sigmoidoscopy, a colonoscope is a much longer and more complicated instrument, which could visualize the entire colon tract and remove abnormal tissues during one examination. The doctor can examine the inside of the colon closely. Special instruments can be inserted through the colonoscope to remove any suspicious tissues such as polyps if necessary. Before the endoscopic test, bowel preparation is necessary so that the doctor can view the inner linings during the test. The colonoscopy test usually lasts for about 30 minutes, but it may take longer time if abnormalities are found and removed. If the doctor finds a

larger polyp or any abnormal tissue else, biopsy usually can be conducted. Colonoscopy is accepted as the routine tool for the diagnosis of colorectal cancer or adenomatous polyps (Anderson 2011).

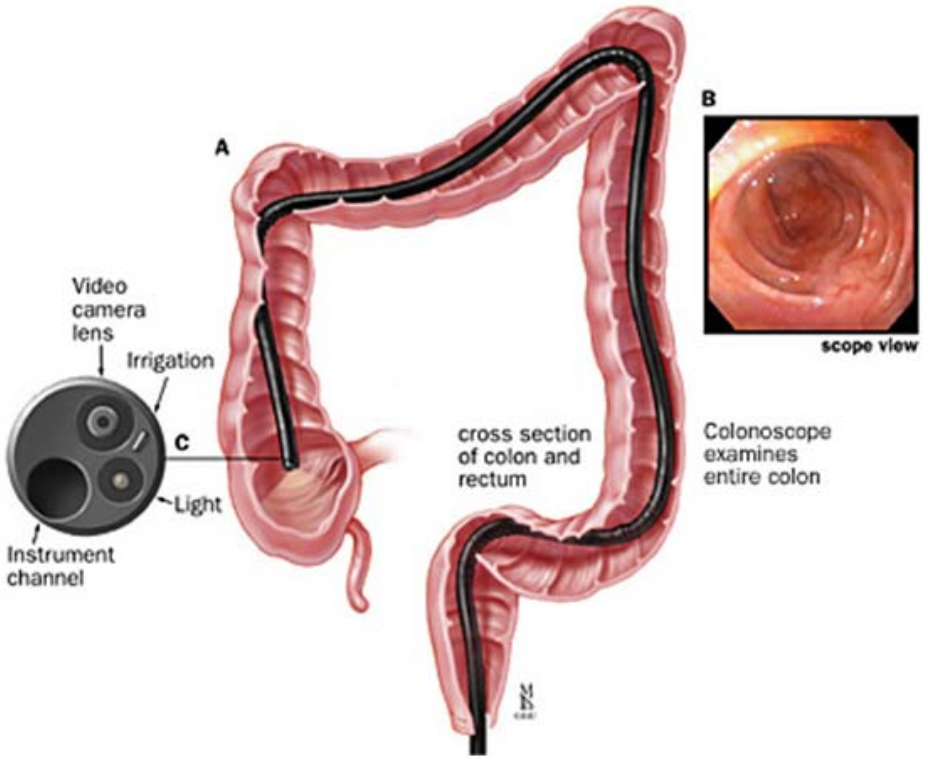

Figure 2.4.Diagram of Colonoscopy (Colorectal Cancer Center, Johns Hopkins Medicine)

http://www.hopkinscoloncancercenter.org/JHH_Home.aspx?CurrentUDV=59

2.4.3 Barium Enema with Air Contrast

Barium enema with air contrast, which allows examination of the complete colon, is also called double-contrast barium enema (DCBE) or air-contrast barium enema. Basically this test is kind of X-ray test. Barium sulfate is usually allowed to spread throughout the colon and to partially fill the colon. Air is then used to outline the inner

part of the colorectal tract to detect abnormal areas on X-ray. If suspicious areas are found in this test, a colonoscope will be done for further exam. Before the test, it is essential to empty the colon and rectum so that the doctor can see them during the test. The procedure usually takes about 30 to 45 minutes. X-ray pictures of the lining of the colon are taken, which allows the doctor to detect polyps or cancers. The patients may be asked to change to different positions so that different perspectives of the colorectal tract can be shown on the X-ray. If any suspicious areas are found in this test, a colonoscopy will likely be done to remove them or to exam closely. This method is much less sensitive than colonoscopy for detecting small abnormalities (Anderson 2011).

2.4.4 Computed Tomography Colonography (CTC)

Computed Tomography Colonography (CTC), which is also called virtual colonoscopy, is a type of computed tomography (CT) scan of the colon and rectum. Instead of taking one picture, CT scanner takes many pictures as it rotates around the patients. A computer then processes all the pictures into image sequences of the part of the body being studied. CTC could provide cross-sectional 2- or 3- dimensional information of the entire colorectal tract which allows detecting polyps or cancer. Before the test, it is also important to empty the colon and rectum. CTC is a non-invasive screening technique, which usually takes about 10 to 15 minutes. This test also exposes the patient to a small amount of radiation. Studies have shown that the performance of CTC is similar to that of colonoscopy regarding the ability of detection of invasive cancer and polyps approximately 1 cm or larger in size (Anderson 2011).

2.4.5 Magnetic Resonance Imaging (MRI)

MRI is known as a non-hazards imaging tool on human beings and could provide excellent soft tissue imaging capabilities. Compared with CTC which produces radiation exposure, MRI is more popular for colorectal cancer diagnosis. MRI can be used to accurately measure the spread of tumor in the surrounding mesorectum, and to assess the circumferential resection margin between the edge of tumor and the fascia recti (Brown et al., 2003). MRI could provide cross-sectional images of the colon and rectum without radiation hazards, and the entire abdominal pathology. Generally MRI is accepted as the gold standard exam in the staging of rectal cancers. Due to the excellent soft tissue imaging capabilities and advanced imaging processing techniques, three-dimensional images can be obtained. The technique of MRI colonography is also developing. However, it is limited by long acquisition time and a high risk of motion artifacts. And it is also not sensitive enough (79%) to the early tumor (T stage) (Kwok et al., 2000).

2.4.6 Endoscopic Ultrasound (EUS)

EUS is widely used in clinical application due to its ability to evaluate the structure alteration on the colorectal wall and nearby organs. EUS does not produce any radiation exposure. EUS is good at imaging soft tissues which makes it suitable for clinical and research studies of colorectal cancer. It is especially valuable to detect the inflammation in GI tract, where wall thickens, wall morphology changes or surrounding lymph nodes change. Endoscopic ultrasound (EUS) using endoscopic ultrasound probes allowing

high-resolution imaging of the colorectal wall layers. Wall layers can be visualized using high-frequency endoscopic ultrasound transducer. By applying special techniques, such as Doppler imaging, contrast agents, additional information can be obtained. Qualitative and quantitative information of colorectal wall can be obtained by applying EUS. However, most of the current applications are focused to guide other interventional operations based on its high-resolution overall structure image. Early-stage cancer detection or *in situ* characterization of abnormal tissues is challenging for EUS because its image contrast mechanism relies on bulk mechanical properties (Kelly et al 2001).

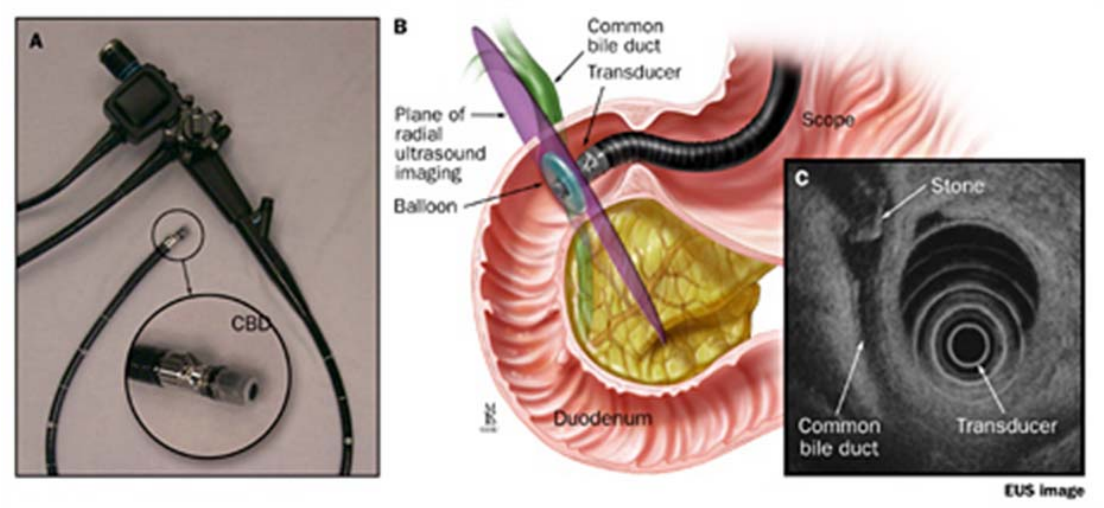

Figure 2.5.Diagram of Endoscopic Ultrasound (EUS)
(http://www.alinastoita.com/procedures/endoscopic-ultrasound-eus/)

2.4.7 Faecal Occult Blood Test (FOBT)

The FOBT can detect very small amount of blood in stool (blood that is non-visible with the naked eye). The blood vessels surrounding the larger colorectal abnormalities,

such as polyp and cancer, are usually fragile and easily damaged by the feces. A small amount of blood is usually released into the feces from the damaged vessels. The FOBT test could detect blood in the stool by a chemical reaction. This test cannot tell the actual position and cause of the blood. If the result is positive, a colonoscopy is necessary to find out the cause of the bleeding. This FOBT screening test is done by a kit so that the patient could use it at home that allows the patient to check more than one stool sample. Before the test, some foods or drugs are not allowed because they may affect the test. Bleeding in colorectal tract may be undetectable, so accurate test may require repeated testing that consists of collecting several samples from consecutive bowel movements (David et al., 2010). It has been shown that the use of this method may reduce the risk of death from CRC by 15% to 33% (Osborn et al., 2005). The effectiveness of FOBT is highly dependent on repeated screenings over time (Nabil and Thomas, 2011).

2.4.8 Stool DNA (sDNA) Test

sDNA test detects certain abnormal DNA sections from cancerous tumors and large polyps in stool samples instead of looking for blood in stool. Colorectal cancer cells often contain DNA mutations in certain genes. Cells from colorectal abnormalities, such as cancers or polyps, containing these mutations are usually shed in the stool. This sDNA test is much more expensive than other types of stool tests. The sDNA test doesn't require any special bowel preparation. But if the result is positive, a colonoscopy test will be conducted. Unlike FOBT, although it only requires a one-time

collection, special designed cooling pack is necessary for temperature control during shipping. (Anderson 2011).

2.5 RESEARCH GAP

Colorectal cancer may take many years to develop and early diagnosis of colorectal cancer may greatly improve the opportunities of a complete cure. The U.S. National Cancer Policy Board of the Institute of Medicine has estimated that even the modest efforts to implement screening methods for colorectal cancer would result in a 29% drop in cancer deaths in 20 years (Jemal et al 2010).

Diagnosis of cases of colorectal cancer through screening tends to occur 2–3 years before diagnosis of cases with symptoms (Cunningham et al., 2010). At least 80% of colorectal cancers arise through localized cancers or premalignant adenomas (David, 2010). Thus, screening has the potential to reduce colorectal cancer deaths by 60% (Efron, 2011). Early detection is necessary to decrease CRC-related mortality; because early stage disease shows good prognosis and later stages have poor survival rates (Hayat, 2009). If colorectal cancer is treated in early stage, minimally invasive surgery as a treatment that can reserve the maximum colon function is more acceptable to the patient.

Regular screening is encouraged for detection and removal of pre-cancerous growths and the diagnosis of malignancies at earlier, more treatable stages (Jemal et al 2010). Current screening methods include stool examination (fecal occult blood test, M2-PK) to check blood or chemical marker for abnormality, endoscope (colonoscopy, sigmoidoscopy), computed tomography (CT) based virtual colonoscopy, digital rectum

exam (DRE), etc (Atlanta: American Cancer Society 2011). If an abnormality is detected by any of these methods, a standard colonoscopy examination will be required to perform, during which biopsy may be conducted. Removed samples are microscopically evaluated to determine the presence or to check the spread of cancer. Although biopsy is a gold standard to confirm malignancy, the detection of abnormality during colonoscopy examination only relies on doctor's experience. Thus, doctors tend to over-biopsy to reduce the chance of missing malignant tumors. Furthermore, to determine cancerous area and a safe surgical margin, patients typically undergo excessive biopsies with significant discomforts and a prolonged examination time.

A number of methods are available for detecting CRC at an early stage. A method compatible with endoscope with high sensitivity and specificity may significantly help doctors to precisely detect and accurately diagnose colorectal abnormality, and reduce unnecessary biopsies and cancer spread.

CHAPTER 3 DEVELOPMENT OF A NOVEL HIGH-FREQUENCY ENDOSCOPIC ULTRASOUND SYSTEM

3.1 INTRODUCTION

In this chapter, I demonstrate the development of a novel high-frequency EUS system that can support an easy fusion with other techniques to improve the sensitivity and specificity for early stage CRC diagnosis. Such EUS system works through the accessory channel of a standard endoscope with a mechanical side-view high-frequency single element ultrasound transducer. The electronic system employed a FPGA as the core microprocessor to implement flexibility, diversity, and real-time applications. Large SNR and high precision data acquisition were obtained by using low noise electronics. High speed PCIE interface was implemented in this system for real time transmission. To achieve compact and cost-effective implementation, the system design is based on electronic components and PCB. In addition, this EUS system has achieved reconfigurable hardware circuitry, programmable processing algorithms, flexible imaging control and raw radio frequency (RF) data acquisition. Lastly, phantom test, *ex vivo* imaging of swine, mouse and rabbit colon specimen, and *in vivo* imaging of rabbit were conducted to evaluate the performance of the system.

3.2 EUS SYSTEM DESIGN

A novel high-frequency EUS system was developed for colorectal cancer diagnosis. The system block diagram is illustrated in Figure 1. One-dimensional depth resolved ultrasound signals were transmitted and received with a miniaturized side-view single element endoscopic ultrasound transducer. Cross-sectional side-view images are produced by rotating the endoscopic ultrasound transducer with a smart motor. An integrated pulser/receiver was implemented in printed circuit board (PCB) for compact and cost-effective design. The pulser generated high voltage short pulses at desired frequency and spectrum specifications to excite the transducer. The receiver processed echo signals by a FPGA-based high speed digital receiver, which incorporated the front-end electronic modules including amplifier, filter, analog-to-digital converter (ADC), FPGA microprocessor and PCIE interface. Images and data are displayed and stored in a PC for further investigations (Qiu et al. 2012c). The details of this EUS system are described in the following sections.

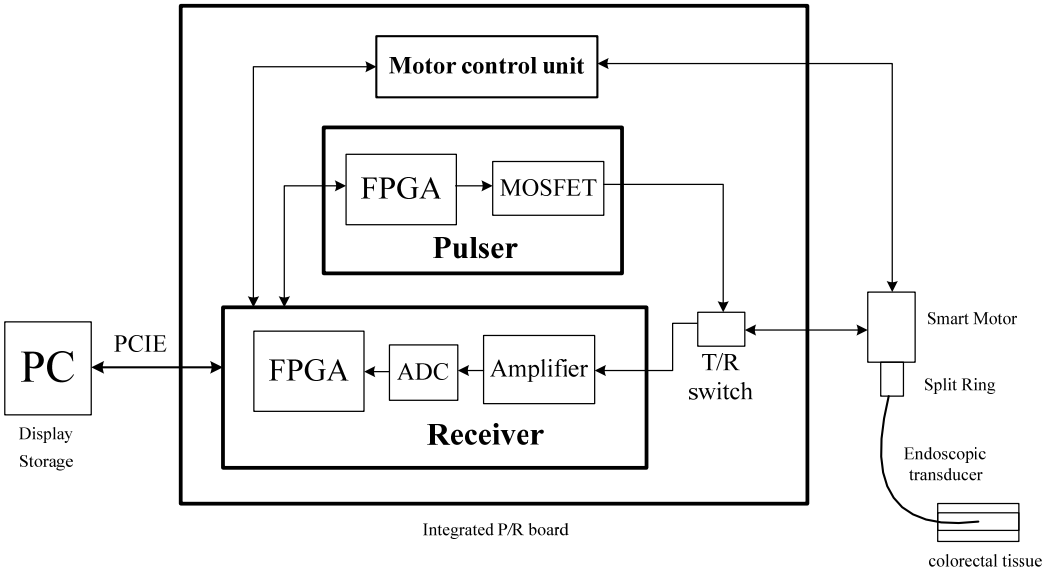

Figure 3.1.Block diagram of novel high-frequency EUS system

3.2.1 Endoscopic Ultrasound Transducer

A 30.5 MHz single element side-view endoscopic ultrasound transducer was fabricated using PMN-0.28PT single crystal which was supported by our cooperators from Department of Applied Physics of The Hong Kong Polytechnic University. Conductive epoxy (E-solder 3022, Von Roll Isola, New Haven, CT) was casted onto the single crystal as the backing layer to eliminate the back reflection and reduce the ring-down of the transducer. Parylene C was evaporated onto the transducer surface by a parylene deposition system (model PDS 2010, Specialist Coating System) and used as the matching layer to compensate the acoustic impedance mismatching between the PMN-0.28PT single crystal and target tissue. The detailed transducer fabrication procedure followed that described by Zhou et al. 2007. A photo of the finished transducer is

shown in Figure 2a. The transducer element was housed in a small stainless steel case with inner and outer diameter of 1.5 mm and 2.0 mm, respectively, as illustrated in Figure 2b. The total length of the flexible cable is 28 cm. The transducer testing was conducted using Panametrics 5900PR pulser/receiver (Olympus NDT Inc., Waltham, MA) and digital oscilloscope (Infinium 54810A, HP/Agilent, Santa Clara, CA). The performance of the transducer, including central frequency, -6dB bandwidth and frequency spectrum, was evaluated in deionized water using a conventional pulse-echo response measurement (Cannata et al. 2003).

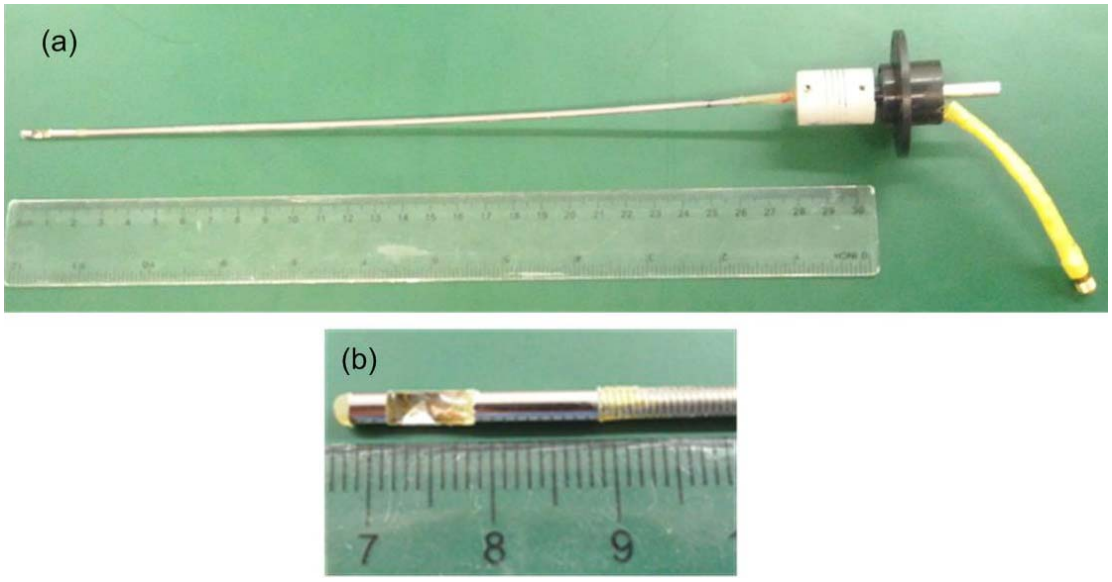

Figure 3.2. (a) Photograph of the single element side-view endoscopic ultrasound transducer (PMN-0.28PT, 30.5 MHz central frequency); (b) The endoscopic ultrasound transducer that includes active element, backing material, matching layer, signal wires and metal housing was fabricated into a flexible stainless tube with inner and outer diameter 1.5 mm and 2.0 mm

3.2.2 Integrated Pulser/Receiver Board

An integrated pulser/receiver board which was developed by our previous group members was implemented for this novel high-frequency EUS system as illustrated in Figure 3. The pulser/receiver employed a high performance FPGA component (Stratix II EP2S60F672C5, Altera Corporation, San Jose, CA) to implement the control of timing and spectrum characteristics of the high voltage short pulse output. Meanwhile, the FPGA also processed the received echo signals with proper algorithms (Sun et al. 2007).

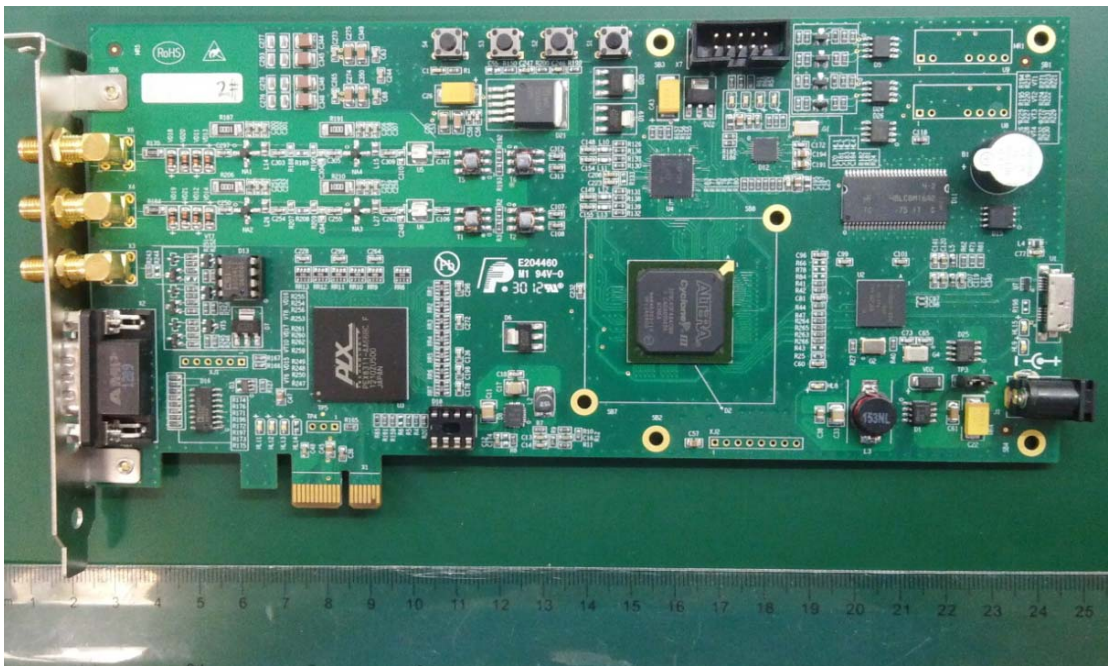

Figure 3.3.Photograph of integrated pulser/receiver board

During transmission, the pulser module was activated to generate high voltage bipolar pulse to excite the transducer with high speed metal-oxide-semiconductor field effect transistor (MOSFET). MOSFET driver (EL7158, Intersil Corporation, Milpitas, CA)

and MOSFET pair (TC6320, Supertex Inc., Sunnyvale, CA) were utilized to accomplish high voltage output.

At reception, the receiver module was turned on to condition and process the echo signals. A low noise preamplifier (SMA231, Tyco Electronics Co., Berwyn, PA) was implemented as the first stage amplifier to achieve large SNR, followed by a second stage amplifier (THS4509, Texas Instruments Inc., Dallas, TX) to obtain adequate amplification gain. A high speed, 11 bits ADC (ADS5517, Texas Instruments Inc., Dallas, TX) with a maximum sampling rate of 200 mega-samples per second (MSPS) was used for signal digitization. After the digitization, the signal was transferred to FPGA through low voltage differential signaling (LVDS) bus. With field programmable technology, different signal processing algorithms such as band-pass filter, Hilbert transform, envelop detection and digital scan conversion (DSC) could be easily programed. A 128M-bit synchronous dynamic random access memory (SDRAM) (MT48LC8M16A2, Micron Technology Inc., Boise, ID) was utilized for temporary data storage. Lastly, the processed images or raw RF data could be transferred to a PC through a PCIE interface component (PEX8311, PLX Technology Inc, Sunnyvale, CA) for display, storage or post-processing (Sun et al. 2008a).

To evaluate the system performance, the gain was first measured by inputting a small sinusoidal signal to the system produced by a function generator (AFG 3251, Tektronix Inc., Beaverton, OR), while outputting the signal to an oscilloscope (and a digital oscilloscope (LeCroy wavepro 715Zi, LeCroy Corp., Chestnut Ridge, NY). The ratio of the amplitude of the output over the input sinusoidal signals defines the gain at a specific frequency. Such a measurement was performed over a wide frequency range,

and the system linearity and gain flatness was obtained subsequently. Secondly, the noise level of the system was tested by measuring the minimum detectable signal level and dynamic range. Five-cycle sinusoidal signal which was produced by a function generator was attenuated by a sets of attenuators and transferred to the high-frequency EUS system. After the front-end electronics, the minimal amplitude of the weak signal which could be identified from the background noise represented the minimum detectable signal level. The dynamic range was obtained from the gain and the minimum detectable signal level.

The signal processing algorithms were performed by the on board FPGA chip. The FPGA could implemented multiple functionalities by programming which were traditionally realized by hardware. Further, those programmed functions could be easily updated by reprogramming the FPGA algorithms without changing hardware. Therefore, the FPGA could significantly contribute to the flexibility and diversity performance of the system. A double data rate LVDS buffer was used to decode the digitized ultrasound echo data through high speed ADC. Both the rising and falling edges of clock were employed for data transferring to achieve high data throughput. A band-pass filter (BPF) which was based on finite impulse response (FIR) structure was used to remove noise from spectrum of interests. The coefficient of the BPF was reconfigurable to match transducers with different center frequencies and bandwidths. After filter, the signal was then transferred to an envelope detector to achieve envelope extraction by Hilbert transform algorithm. The acquired envelope data would then pass through digital scan conversion and logarithmic compression for coordination conversion and data compression, respectively. A flexible scan converter which was based on linear

interpolation was utilized to achieve fast and accurate processing. Lastly, image data was sent to a PC through PCIE interface for display and storage. A SDRAM controller module was employed with external SDRAM to achieve flexible digital scan conversion and logarithmic compression (Qiu et al. 2012a, Sun et al. 2008b, Sun et al. 2009).

3.2.3 Smart Motor

To acquire two-dimensional (2D) cross-sectional view, the single element transducer was rotated by a smart motor (MOOG ANIMATRICS', Silicon Valley, USA). The smart motor could communicate with the ultrasound system by the control interface on PC. The rotary speed of the smart motor is set to 300 rpm and 5 frame/s RF data could be transferred to PC. A split ring is employed to connect the flexible endoscopic ultrasound transducer with the smart motor.

3.3 PHANTOM TEST

A tissue-mimicking phantom was made with deionized water, high-grade agarose, preservative, propylene glycol, filtered bovine milk, and glass-bead following the procedure by Madsen et al. 2010. The phantom mimicked the attenuation and backscattering of soft tissue to assess this EUS systems performance. A whole was made in the center of the phantom to accommodate the EUS transducer. Images of the phantom were acquired, and contrast to noise ratio (CNR) was calculated subsequently.

3.4 ANIMAL EXPERIMENTS

The animal experiments were conducted in the Centralised Animal Facilities of the Hong Kong Polytechnic University under a protocol approved by the Department of Health, The Government of the Hong Kong Special Administrative Region and the university's Animal Subjects Ethics Sub-committee.

3.4.1 *Ex vivo* Imaging of Colon Specimen

a. A swine colon tissue was purchased from the market. It was cleaned and prepared using pure water before experiment.
b. An ICR mouse at 5 months old, weighting 25 gram, were acquired and housed at CAF of the Hong Kong Polytechnic University, and sacrificed right before the experiment. A 5cm segment of cecum between the appendix and the ileo-cecal valve was rapidly excised.
c. A New Zealand male white rabbits at 5 months old, weighting 2.5 kg, were purchased from CAF of the Chinese University of Hong Kong and housed at CAF of the Hong Kong Polytechnic University. The rabbits were fasted for 24 hrs before the experiment and sacrificed at the start of the experiment. A segment of 5cm of descending colon was rapidly excised.

After the colon tissue specimen was acquired, they were immersed in 0.9% saline at room temperature. The endoscopic ultrasound transducer was then inserted into the colon tissue, and EUS images of the tissue specimen were acquired and stored in a PC.

3.4.2 *In Vivo* Imaging of New Zealand White Rabbit

One New Zealand male white rabbits at 4-5 months old, weighting 2.5-3 kg, were acquired from CAF of the Chinese University of Hong Kong and housed at CAF of the Hong Kong Polytechnic University with normal diet. Prior to the experiment, the rabbits were fasted for 24h. The rabbits were anesthetized with injection of 35 mg/kg ketamine and 5 mg/kg xylazine via IM (Flecknell 1996). Rabbits were kept at a dorsal position with their legs and arms fixed. A 10cm long sterilized plastic hollow pipe with an outer & inner diameter of 3.5 mm & 3 mm was inserted into the anus to brace the colorectal tract. Sterilized coupling water was introduced into the rectum by syringe. *In vivo* EUS scan was carried out with the high frequency endoscopic transducer inserted into the colorectal tract. The rabbits were allowed normal diet after recovery from anesthesia.

How to couple the ultrasound transducer and animal colorectal tract is the main concern for the in vivo experiment setup. Clinically, the coupling medium is pure water and there is sealed tube filled with oil surrounding the transducer to protect the transducer and couple the transducer with the tube. According to our testing, the high frequency ultrasound echoes of our ultrasound platform attenuate sharply through tube material for low-frequency ultrasound transducer. After a period of testing, I have customized one kind of ultra-thin transparent material as our transducer tube. Photograph 2 shows the process of tube acoustic attenuation test. Photograph 3 shows the performance of the ultra-thin transparent tube. This tube was customized by us and produced at Shanghai.

3.4.3 Histology

Once the imaging scan was complete, the colon tissues were cleaned, and fixed in 4% formaldehyde during 16 hours for paraffin wax embedding. The paraffin-embedded tissues were cross-sectioned (5mm) stepwise transversally to the colon's longitudinal axis and stained with hematoxylin and eosin (H&E).

3.5 RESULTS

The photograph of the novel high-frequency EUS system working for *in vivo* experiment is shown in Figure 3.4. It included PC with integrated pulser/receiver board, EUS transducer, smart motor, motor power supply and PC screen.

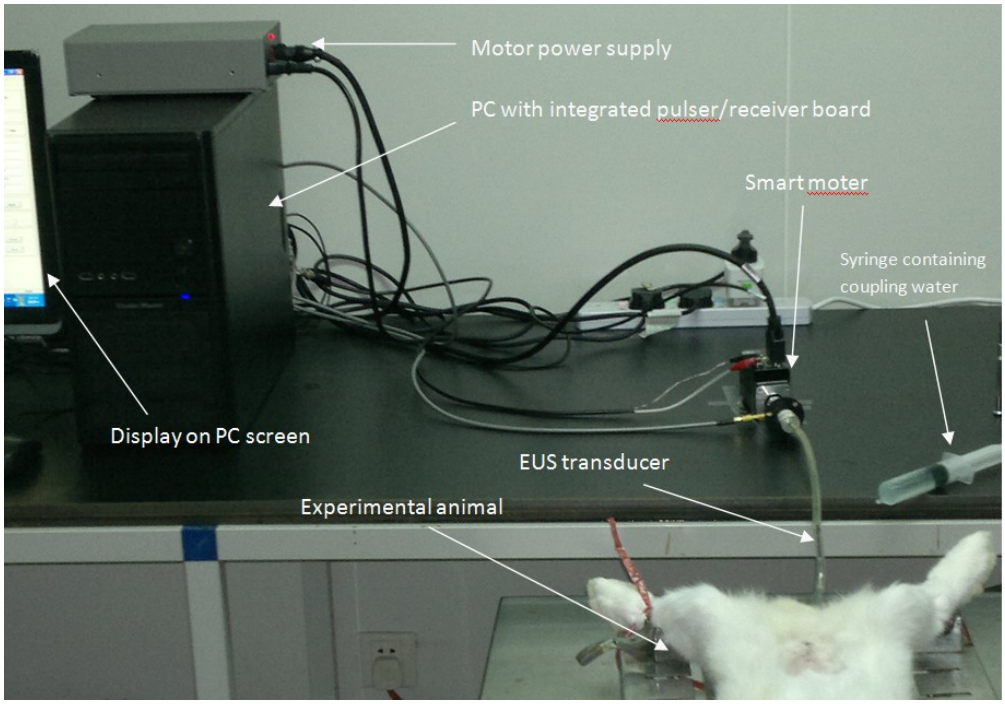

Figure 3.4.Photograph of the EUS system for an *in vivo* rabbit experiment.

Figure 3.5 shows the measured pulse-echo waveform and frequency spectrum of the in-house made single crystal EUS transducer (PMN-0.28PT, 70μm thick, 0.9 mm × 0.9 mm). It indicated that the transducer had a central frequency of 30.5 MHz with -6dB bandwidth of 30.7% (lower frequency 25.9 MHz, upper frequency 35.2 MHz). The electronic performance of the integrated pulser/receiver board is summarized in Table 3.1. The pulser module could output a bipolar pulse with maximum amplitude of 160Vpp and adjustable central frequencies. The front-end electronics of the receiver module could reach a maximal gain of 47dB with good linearity at a maximum fluctuation of less than ±1.2dB between 10MHz and 90MHz. The receiver module of the system could detect a minimal signal of less than 25μV. The dynamic range could achieve 51dB at central frequency of 35MHz. The resource utilization of the FPGA is shown in Table 3.2. Large amount of FPGA resources were saved in order to support the combination of the EUS imaging with other techniques to form a multi-modality diagnosis. High speed imaging algorithm by pipe-line signal processing was implemented in FPGA. The data transferring speed could reach more than 150MByte/s by PCIE interface. The frame rate was up to 200 frames per second for PCIE (frame size of 512×512 pixels) (Qiu et al. 2012b).

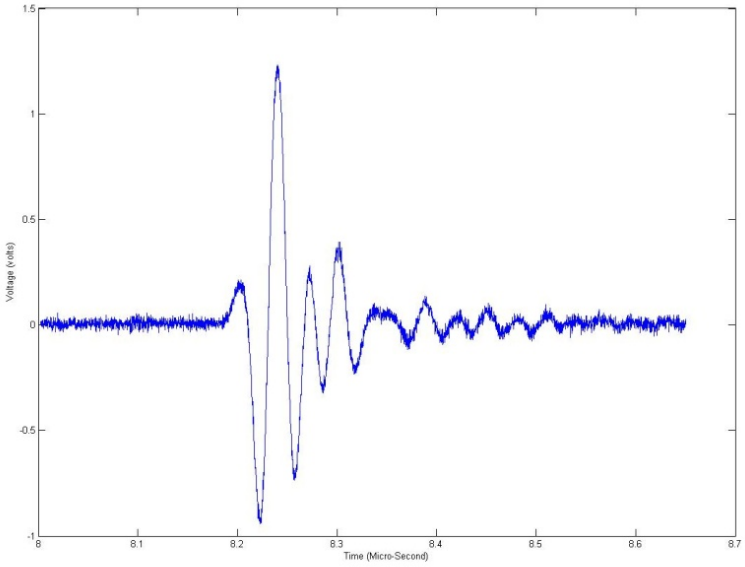

(a)

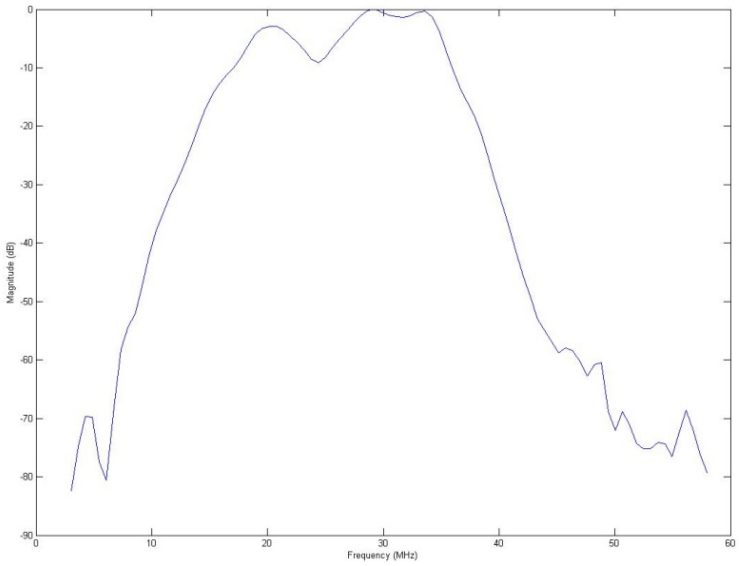

(b)

Figure 3.5.EUS transducer pulse/echo measurement. (a) pulse/echo waveform and (b) frequency spectrum with 30.5 MHz central frequency, 30.7% -6dB bandwidth (with lower frequency 25.9 MHz and upper frequency 35.2 MHz).

Table 3.1. Electronics performance of the system specs

Articles	**Performance**
Frequency range	20-100MHz
High voltage tunable pulse	Up to 120V Vpp
Gain	45dB
Gain fluctuation	±1.4dB
ADC	11bits, 200MSPS
Minimum detectable signal	25μV
Dynamic range	57dB
Software improved dynamic range	59.9dB
Data transmission speed	150MByte/s (PCIE)

Table 3.2. Utilization of FPGA resource

Articles	**Resource utilization**
Adaptive look-up tables (ALUTs)	5340 (11%)
Pins	237 (48.4%)
DSP block 9-bit elements	64 (22%)
Memory bits	63782 (3%)
PLLs	3 (49%)

3.5.1 Phantom Test

The image acquired on tissue-mimicking phantom is shown in Figure 3.6. The result demonstrated that the calculated contrast to noise ratio (CNR) of the tissue phantom was higher than 1.1 in the range of 2.0 to 5.0 imaging depth (Filoux et al 2011), and penetration depth of the novel high-frequency EUS system is beyond 5 mm the thickest part of the phantom which is adequate for early CRC applications. The phantom image result also showed that the system has low system noise and good image performance.

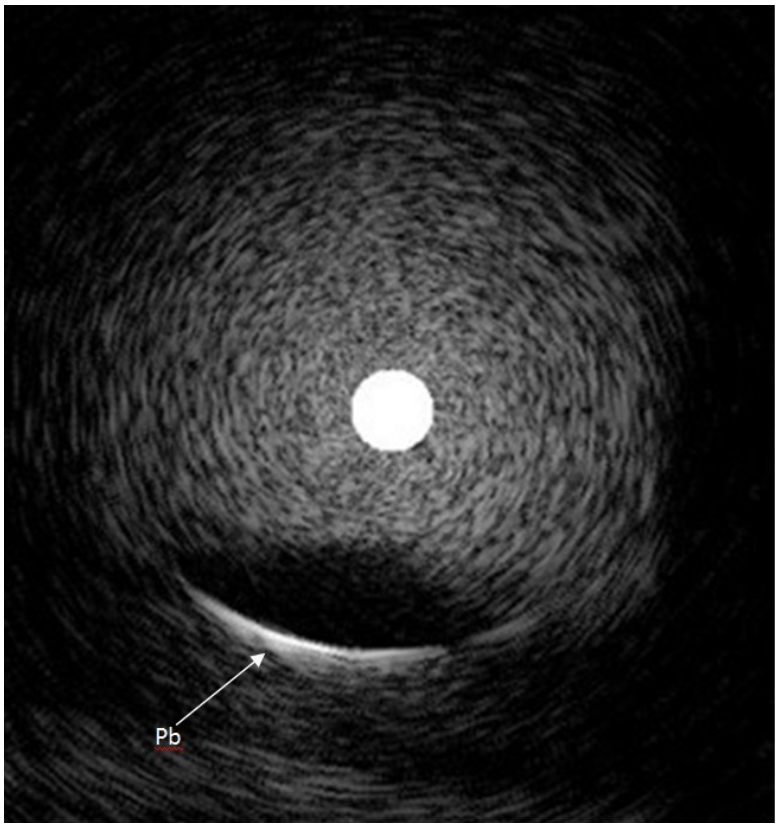

Figure 3.6. Tissue phantom image acquired by the high frequency EUS system with EUS transducer at the center, phantom surrounding the transducer, and hyperechoic reflection from the surface of plastic box (Pb) container.

3.5.2 Animal Experiments

Ex vivo Imaging of ICR Mouse Colon

The ultrasound image of *ex vivo* normal ICR mouse colon is shown in Figure 3.7 (a). The EUS image displays the EUS transducer at the center of the lumen and the hyperechoic mucosa (Mu) layer, a second hypoechoic layer corresponding to the muscularis mucosae (Mm), a third hyperechoic layer submucosa (Sm), a fourth

hypoechoic layer muscularis propria (Mp), and fifth hyperechoic layer adventitia (Ad). The layers identified in the EUS image are well correlated with five layered structures shown in the histology Figure 3.7 (b). The image result showed that the system is able to delineate normal superficial layers of mouse colon with hyper- and hypo-echoic layers.

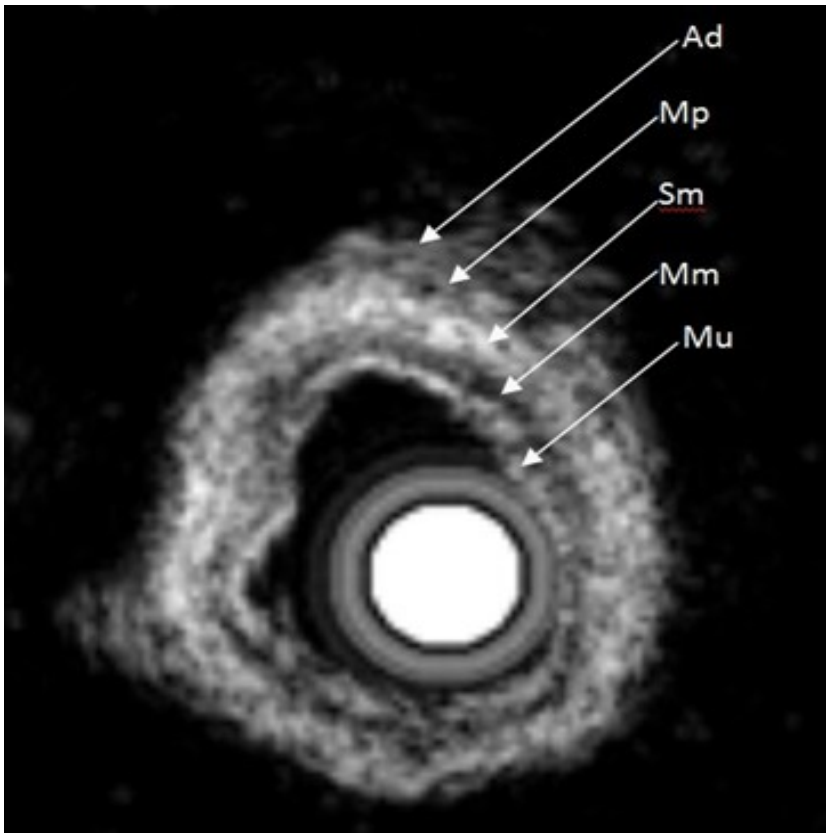

(a)

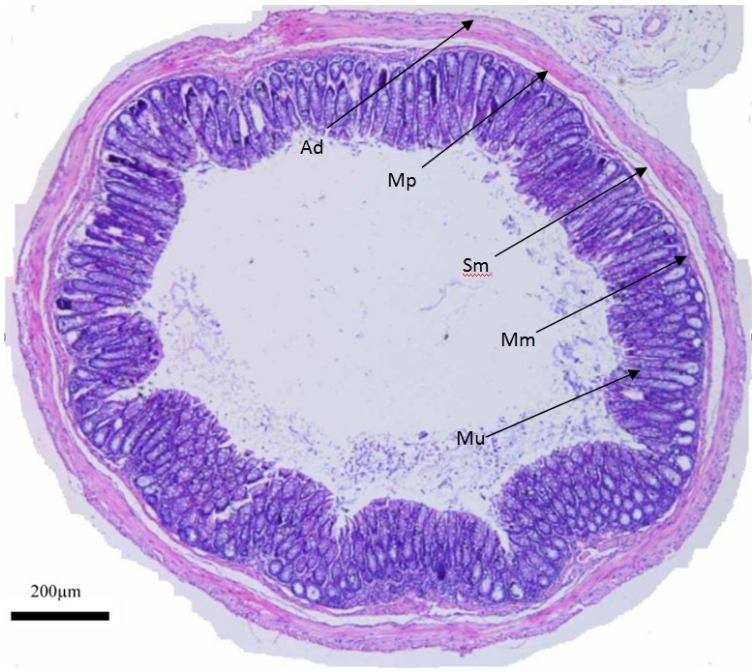

(b)

Figure 3.7. (a) *Ex vivo* EUS image obtained from a segment of a normal ICR mouse colon and (b) the corresponding hematoxyylin and eosin (H&E) stained histological picture (50 × magnification). The EUS image displays the EUS transducer at the center of the lumen and the hyperechoic mucosa (Mu) layer, a second hypoechoic layer corresponding to the muscularis mucosae (Mm), a third hyperechoic layer, submucosa (Sm), a fourth hypoechoic layer muscularis propria (Mp), and fifth hyperechoic layer adventitia (Ad) The layers identified in the EUS image are well correlated with five layered structure in histology.

Ex vivo Imaging of New Zealand Rabbit Colon

The ultrasound image of ex vivo normal New Zealand White rabbit colon is shown in Figure 3.8 (a). The EUS image ex vivo also displays 5 layered structures from the hyperechoic mucosa (Mu), to hypoechoic muscularis mucosae (Mm), hyperechoic submucosa (Sm), hypoechoic muscularis propria (Mp), and hyperechoic adventitia (Ad).

It also well correlated with five layered structure in histology Figure 3.8 (c).

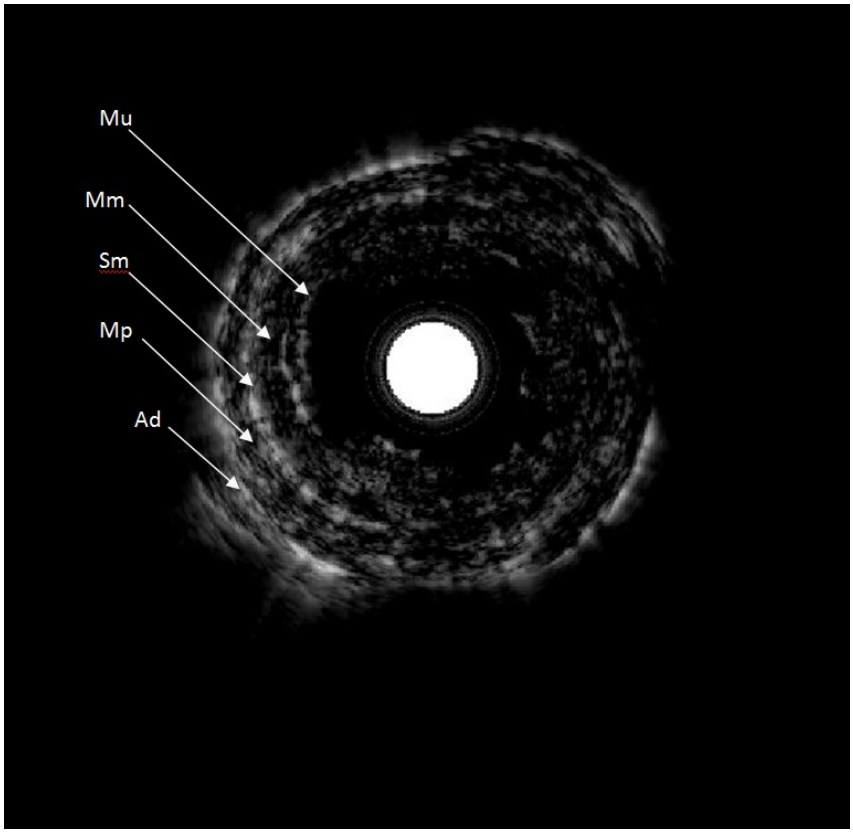

(a)

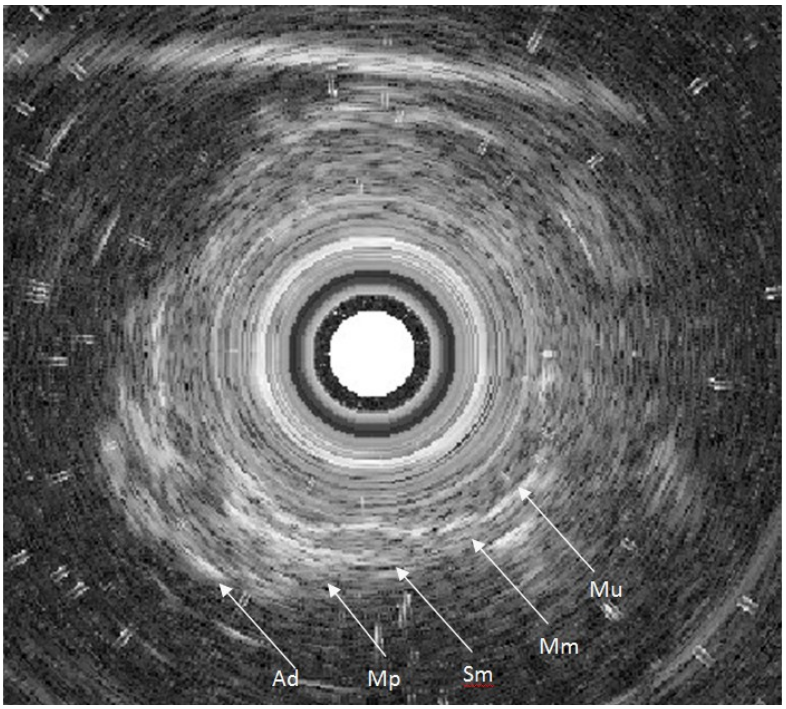

(b)

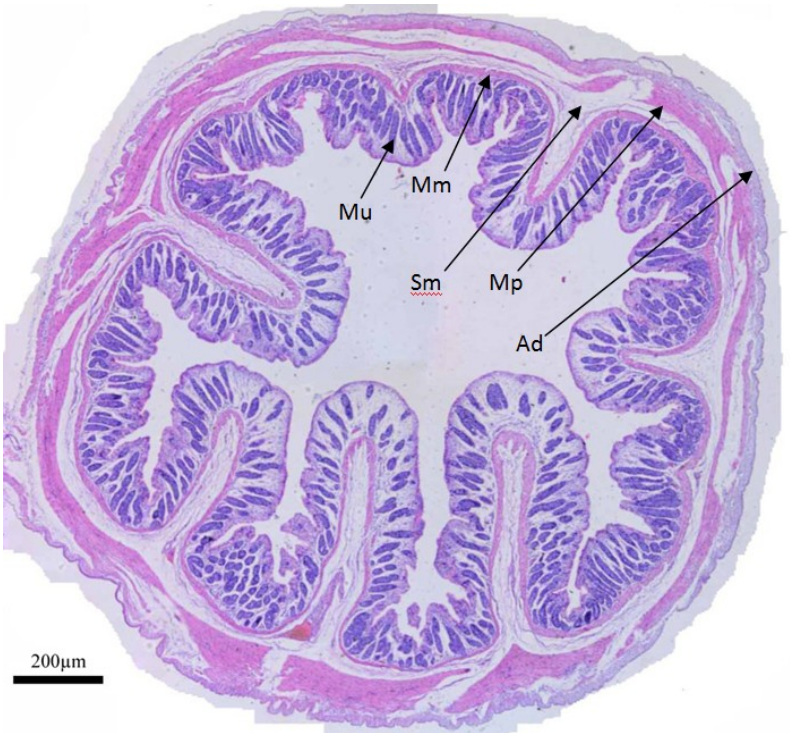

(c)

Figure 3.8. (a) EUS image obtained ex vivo from a normal segment of a NZW rabbit colon; (b) EUS image obtained in vivo from a normal segment of a NZW rabbit colon; (c) the corresponding hematoxyylin and eosin (H&E) stained histological picture (50 × magnification). The EUS image ex vivo and in vivo display the EUS transducer at the center of the lumen and the hyperechoic mucosa (Mu) layer, a second hypoechoic layer corresponding to the muscularis mucosae (Mm), a third hyperechoic layer, submucosa (Sm), a fourth hypoechoic layer muscularis propria (Mp), and fifth hyperechoic layer adventitia (Ad) The layers identified in the EUS image are well correlated with five layered structure in histology.

In Vivo Imaging of New Zealand Rabbit Colon

The ultrasound image of in vivo normal New Zealand White rabbit colon is shown in Figure 3.8(b). The EUS image in vivo displays the EUS transducer at the center of the lumen and the hyperechoic mucosa (Mu) layer, a second hypoechoic layer corresponding to the muscularis mucosae (Mm), a third hyperechoic layer, submucosa (Sm), a fourth hypoechoic layer muscularis propria (Mp), and fifth hyperechoic layer adventitia (Ad) The layers identified in the EUS image are well correlated with five layered structure in histology in Figure 3.8(c). Compared with the *ex vivo* experiment result, the *in vivo* experiment result showed more noises because of the air bubbles in the coupling gel produced by the rotating transducer and breathing noise produced by the live animal.

All stained sections of animal tissues were analyzed using light microscopy and compared to the ultrasound images, as shown in Figure 3.7 (b) and Figure 3.8 (c).

Figure 3.7 and Figure 3.8 depict the layered colorectal tract structure of normal ICR mouse and New Zealand Rabbit by high-frequency EUS and the corresponding histology. The center of the lumen is occupied by the high-frequency EUS probe, represented by a gray circle that is surrounded by a bright area corresponding to the ultrasonic pulses multi-reflected between the transducer and the catheter wall. The innermost hyper-echoic circular layer is the mucosa (almost no lymphatic vessel), followed by the second hypo-echoic layer corresponding to the muscularis mucosa (lymphatic vessels appear on superficial surface) (Hurlstone et al. 2009,Smith et al. 2010,Kobaek-Larsen et al. 2000). The third hyper-echoic layer is the submucosa (vascular and lymphatic vessels appear). The high-frequency EUS is able to delineate 30 μm differences of the layers in longitudinal direction.

3.6 DISCUSSION

The present work is aiming to establish a novel high-frequency EUS system, which is able to provide enough precise structure image and compatible with other potential functional imaging tools, to delineate the depth- view structure of colorectal tract where an early abnormalities originates and to combine functional information for in vivo real-time patho-physiological histology. Potential outcome from this work will demonstrate the potential of high-frequency EUS combining other functional imaging tool for complementary high-resolution structural and patho-physiological diagnosis. Compared with the other commercial systems, the open strategy and programmable ability of the customized EUS system makes it suitable to implement the routine colonoscopy and

other potential functional tools. The flexible imaging characteristics such as frequency spectrum of the transmitted pulse, parameter of the receiver filter, sampling rate, number of scan line, and length of scan line can be re-configured easily. The raw RF data could also be transferred and stored by the system. Multiple image processing algorithms such as tissue characterization based on ultrasound raw RF data and penetration improvement based on modulated excitation could be achieved on the customized system. Multi-modality imaging combining high-frequency EUS and other functional tools, e.g. Photoacoustic (PAI), are rather potential in the field of colorectal cancer diagnosis. The flexibility and performance of the customized system might make it suitable for various multi-modality imaging research in different biomedical fields.

CHAPTER 4 QUANTITATIVE ULTRASOUND CHARACTERIZATION OF THE COLORECTAL CANCER USING HIGH-FREQUENCY ENDOSCOPIC ULTRASOUND

4.1 INTRODUCTION

In clinical, tumor is largely assessed based on the evidence of morphological changes. According to the American Cancer Society, 90% of localized malignant colorectal tumors at early stages could be cured (Atlanta: American Cancer Society 2011). Obvious morphological changes may not occur at all for colorectal tumors at early stage. Recently, treatment for colorectal cancer has become increasingly differentiated. Patients with early stage colorectal neoplasia limited to the mucosal layer can be cured with endoscopic treatment [ref]. In those with more advanced stages, surgical treatment should be considered. The most popular diagnostic tool for the detection of lesions in colorectal tract, such as polyps, neoplasia and malignant tumor is colonoscopy although it could only visualize the surface of colorectal tract (Atlanta: American Cancer Society 2011). Benign lesions, such as polyps could effectively be cured by endoscopic resection. In contrast, differentiation of malignant tumors which are possible to metastasize to adjacent organs requires patho-physiological information and penetration depth information for accurate lesion staging and treatment strategy. Therefore, complementary information acquired with routine colonoscopy which is able to determine the tissue's patho-physiology and penetration depth through colorectal wall would bring great potential for accurate early detection of colorectal cancer.

The field of knowledge of high-frequency EUS with QUS for early colorectal cancer diagnosis is yet to be fully determined and a reproducible and feasible animal model is appropriate for further development of this novel modality. VX2 CRC Rabbit model is first time used as a model for endoscopic ultrasound imaging according to our knowledge. In this study, I for the first time show the application of high-frequency endoscopic ultrasound (EUS) along with quantitative ultrasound (QUS) to characterize malignant colorectal tumor and benign colorectal tissue in a rabbit model of VX2 colorectal cancer. Our group has developed a novel high-frequency endoscopic ultrasound (EUS) system for real-time EUS and (QUS) imaging of colorectal cancer in previous studies [ref]. In this study the research purpose was to validate the method of RF spectral analysis to distinguish between colorectal cancer (CRC) and benign colorectal tissue based on our novel high frequency EUS system in a rabbit model of colorectal cancer.

4.2 QUANTITATIVE ULTRASOUND

In brief, the method of spectrum analysis extracts parameters from the backscattered RF US signals from local inhomogeneities in tissue. Backscattered echo signals were processed using regions-of-interest (ROI) to yield some QUS estimates associated with tissue microstructure (i.e., effective scatterer size, acoustic concentration, intercept, and slope. The method of quantitative ultrasound (QUS) imaging has been investigated by several groups. The correlation relationship between many spectra parameters and tissue microstructure has been studied in many different applications, such as prostate

cancer (Feleppa et al. 2001, Feleppa et al. 1996, Feleppa 2008), breast cancer (Golub et al. 1993), ocular cancer (Silverman et al. 2003), lymph node metastases from cancers of the breast (Tateishi et al. 1998) and colon (Tateishi et al. 2004, Noritomi et al. 1998, Mamou et al. 2011, Mamou et al. 2010b), liver disease (King et al. 1985), intravascular plaque (Nasu et al. 2006) and hyperthermic lesions (Lizzi et al. 1997b, Silverman et al. 2006) and has also been implemented to perform real-time tissue-type imaging (Feleppa et al. 2001). Thus I suppose that the spectral parameter of scattering signal from colorectal tissue can also show significant difference between cancerous tissue and noncancerous tissue.

4.3 ANIMAL EXPERIMENTS

The experimental protocol was approved by the Institutional Animal Care and Use Committee of HK and satisfied all campus and National Institutes of Health rules for the humane use of laboratory animals.

New Zealand white male rabbits weighing 2.5 kg to 3.5kg will be used for all experiments. The proposed research requires the physiology, anatomy and size of this species. This species is also the accepted animal model for the research purpose. Animals will be housed one per cage and fed with a commercial pellet diet with free access to tap water.

4.3.1 Rabbit Model of Colorectal Cancer

Currently, experimental animal models of colorectal carcinoma are often induced by chemical carcinogens. This kind of modelling method requires lots of time and the individual variations could be very large. In this experiment, we choose VX2 cell line which is the only tumor cell line for rabbit of unspecified tissue origin to inoculate into rabbit rectum.

VX2 tumor cell line was originally from a Shope virus induced papilloma of the rabbit in 1940 by Kidd and Rous. Since then VX2 has been widely used for various in vitro and in vivo experiments as rabbit tumor model cell line. However, most of the animal models were established in organs with rich blood vessels such as liver and brain. The few successful rabbit rectal VX2 carcinoma models were used to evaluate of radiation treatment of cancers in advanced stage. It has also been noticed that VX2 cell line is not easily obtained from bio-technology companies. Considering the VX2 cell line culture and experiment requirement, the operation skill was supported by Guangdong Provincial Clinical Animal Experiment Center.

4.3.2 Experiments Design

New Zealand male white rabbits at 4-5 months old, weighting 2.5-3 kg were used. Experimental rabbits were lavaged 24h prior to injection surgery. During trans-abdominal tumor cell implantation experiments, rabbits were anesthetized with 30mg/kg pentobarbital sodium via the ear vein. The rabbits would be kept at a dorsal position with their legs and arms fixed. A total of 0.2 mL of suspended VX2 cells were

be injected, followed by injection of 0.1-0.2 mL of normal sodium to fully rinse the VX2 cells into the rectal wall. After about 5 min, the needle was withdrawn slowly. The rabbits were allowed to have normal food following recovery from anesthesia (Joseph et al 1988; Liang et al 2009).

Each group of rabbits were sacrificed by injecting 3.0ml/kg of euthanasia solution T6 in an ear marginal vein (N-[2-(M-methoxyphenyl)-2 ethyl-butyl-(1)]-gamma hydroxy butyramide, 200 mg/ml; 4,4' methylene-bis(cycholexyl) trimethyl-ammonium iodide). A 10cm segment of cecum between the appendix and the ileo-cecal valve was be rapidly excised. Experiments will be carried out with the probe inserted into the colorectal tract. Scans will be conducted simultaneously to identify abnormal tissues. Tumor location, size, activity, circumscription, and metastasis will be determined. The rectum-implanted tumor and the major organs involved would be fixed in formalin embedded in paraffin. Tumor tissue will be cut into sections, stained with hematoxylin-eosin (H&E), and evaluated using a microscope afterwards. The results of in vivo, ex vivo scan and histology will be compared to determine the utility and accuracy of the proposed method (Joseph et al 1988; Liang et al 2009).

4.3.3 Data Acquisition Setup

The colon segment with cancer tissue was immobilized in the scaffold by 4 steel nails, two in head and two in end. The function of the 4 nails was not only to immobilize the colon but also to expand the inner space of the colon to leave enough space for the transducer. The distance between outside scaffold and tissue wall was controlled to

more than 1 cm for avoiding being scanned. Before the scaffold system (Figure 4.1 (a) (b)) was immerged into water, the distances from cancer sites to the head edge of scanned colon were measured and recorded. The recorded distance was used to guide the transducer to cancer position. After the transducer was guided to the designed scan plane, the whole system was started to acquire RF data for further processing.

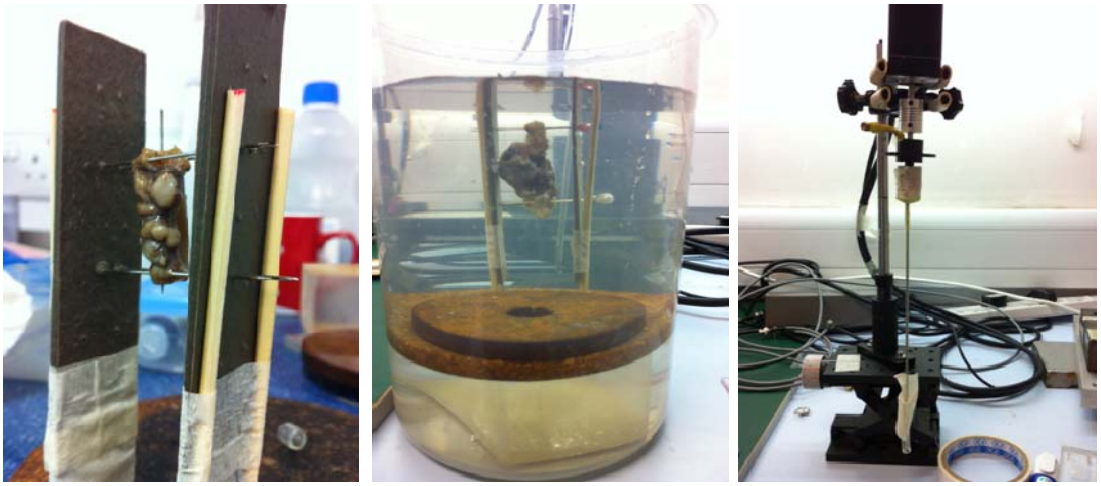

(a) (b) (c)

Figure 4.1. (a) Cancerous colon tissue immobilized in a scaffold; (b) colon tissue immersed in water tank (c) transducer, split ring connection and smart motor

4.3.4 Histological Analysis

Once the imaging scan was complete, the colon tissues were cleaned, and fixed in 4% formaldehyde during 16 hours for paraffin wax embedding. The paraffin-embedded tissues were cross-sectioned (5mm) stepwise transversally to the colon's longitudinal axis and stained with hematoxylin and eosin (H&E). All stained sections of animal

tissues were analyzed using light microscopy and compared to the ultrasound images, as shown in Figure 4.16 (d).

4.4 DATA ANALYSIS

4.4.1 Brief Introduction

I have developed a MATLAB® program. The program could calculate the spectrum characteristics of the region-of-interest and derive multiple ultrasonic spectral parameters to quantitatively analyze the tissue alternations. The details of the method underlying this spectrum technique has been reported previously.

Briefly, the ultrasound data analysis involved in the following five steps: Step 1. Ultrasound B-mode imaging. The conventional B-mode imaging could show the anatomical structure of the tissue. Step 2. ROI delineation. RF echo signals inside the ROI will be gated by a single Hamming window at the same length of the ROI height. Step 3. Spectrum calculation. In order to analyze the RF data within the ROI, each line of the RF data is Fourier-transformed and the power spectrum would be obtained, the resultant spectrum of different N lines is averaged to obtain an ensemble power spectrum of the ROI and is then converted to logarithmic scale. Step 4. Calibration. The averaged 1D power spectrum of the tissue segment will be further calibrated to eliminate the spectrum contribution of the system. A reference phantom calibration method will be used and is described afterwards.

4.4.2 Calibration

To remove spectral contributions associated with the electronic transmitter/receiver and the transducer (Lizzi et al., 1983), calibration is necessary for tissue RF data processing. I selected a glass plane as calibration target because it has significant acoustic impedance difference with water. The back supporter was to insure that the calibration target be vertical to the transducer. Under the target is a marker to record distance between transducer and calibration plane.

In my experiment, the distance was 3mm. 3mm is within the range of the transducer's focal plane; in addition, it is also close to the distance between transducer and colon wall in the vitro experiment. During the calibration process, the transducer is steady instead of rotation because rotating transducer cannot insure it vertical to calibration plane. Yet, the steady transducer may induce single measurement error. To eliminate the error 20 calibration signals was recorded and averaged.

4.4.3 B-Mode Image Construction

B-mode ultrasound images were generated by the received RF signal after series processes including band-pass filtering, envelop detection, dynamic range transformation and median image filter. The final image should be transferred from Cartesian image to Polar image for better understanding using grind and other algorithms. The cutoff frequency was 10 MHz in high pass and 63MHz in low pass respectively. The cutoff bandwidth was slightly wider than the default bandwidth (17.5MHz-32.5MHz) to restore enough backscattered echo information. Dynamic range

was set to be 45; such dynamic range can recover the maximum morphology information and relative low noise. Median filter was applied to eliminate the speckle noise. The order of median filter was evaluated by the tradeoff between residual speckle noise and image quality. Finally, order 3 median filter was found to have the best balance between residual speckle noise and image quality. The normal clinical used B-mode images (Figure 4.2. & Figure 4.3) were generated to demonstrate the tissue morphology. Such image is in polar coordinate with the original point in center refer to the transducer position.

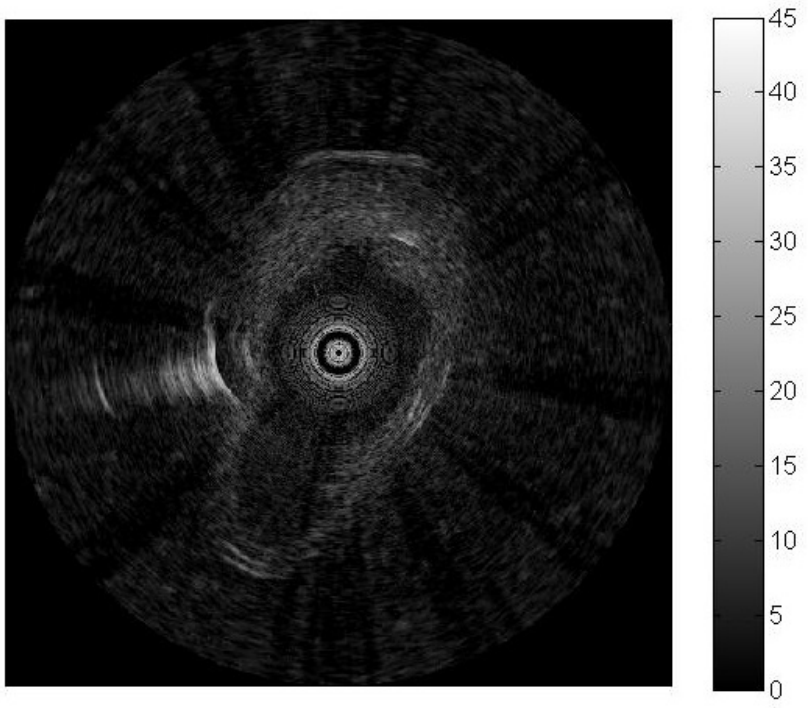

Figure 4.2 B-mode image of colon segment with cancer in polar coordinate.

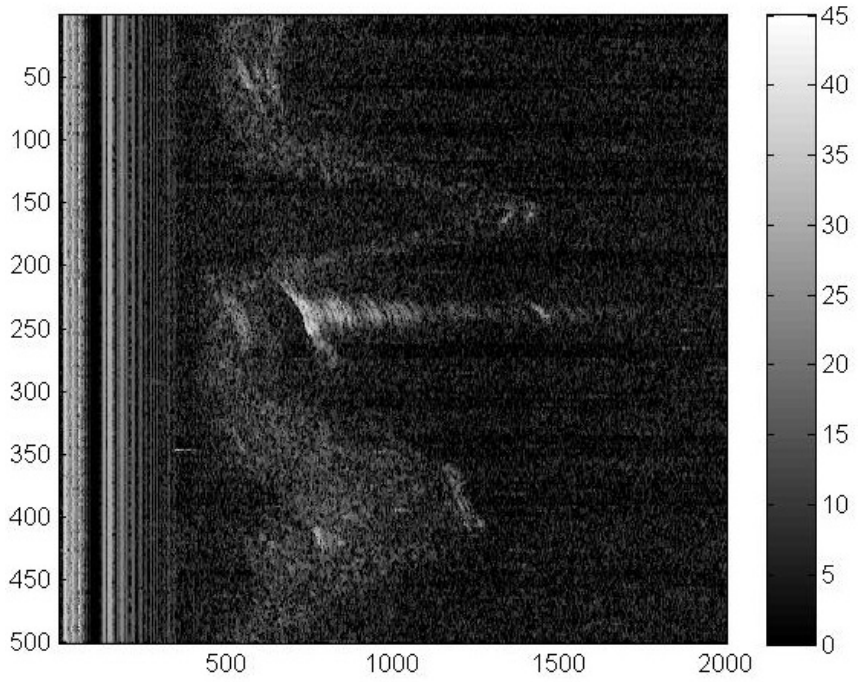

Figure 4.3. B-mode image of colon segment with cancer in Cartesian coordinate

4.4.4 Classification

To develop the database of spectral parameter, the backscattered RF signal was classified into two group, normal tissue group and cancer tissue group. Regions of interest (ROI) from each scan plane was selected and recorded in data pool for further calculation as shown in Figure 4.4. ROI size was standardized to be 0.63mm with 30 scan lines. Totally 90 ROIs of normal tissue were selected from 13 different scanning planes and 79 ROIs of cancer tissue were selected from the same 13 scanning planes.

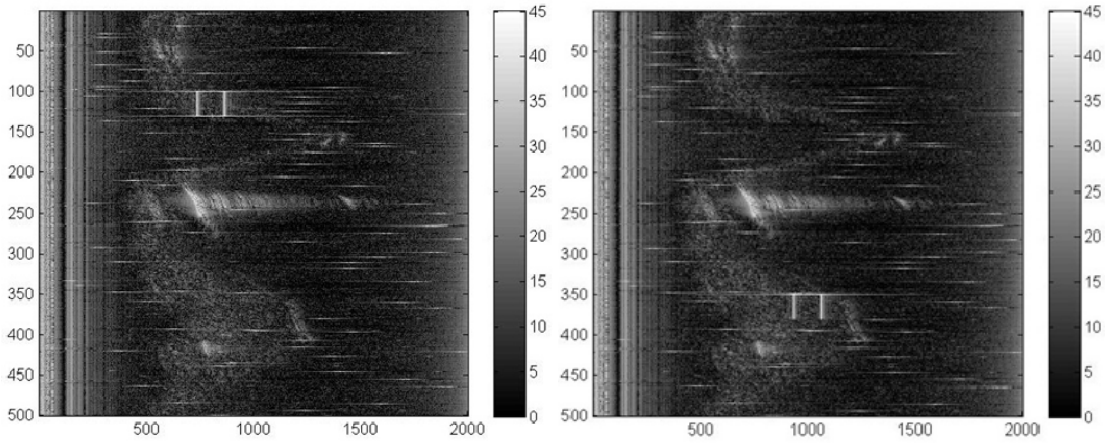

Figure 4.4 ROIs selection in (a) normal tissue region and (b) cancer tissue region

4.4.5 Spectral Parameter Calculation

Three spectral parameters (k, I and M) were derived from the ROI data chosen from the RF data. The RF signal is multiplied by Hanning window of length (L=length of ROI) along each scan line (Lizzi et al., 2009), and then followed by Fast Fourier transformation (FFT). The mean of the squared spectral magnitude was calculated from an ensemble averaged power spectrum in the ROI (Lizzi et al., 2003).

$$S(f) = |FT[RF_L(t)H_L(t)]|^2 \tag{4.5.5.1}$$

$$S_{ROI}(f) = \frac{1}{N}\sum_{i=1}^{N} S_i(f) \tag{4.5.5.2}$$

In eqn (4.5.5.1), the RF signal of ROI is represented as $RF_L(t)$; the Hanning window function of length L is represented as $H_L(t)$. In eqn (4.5.5.2), the averaged power spectrum function of ROI is represented as $S_{ROI}(f)$. The calibrated signal was next calculated by dividing the averaged spectrum by calibration signal. Finally, the calibrated signal was transferred to log form (dB) as:

$$W_{ROI}(f) = 10\log\left[S_{ROI}(f)\right] - 10\log\left[S_{cali}\left(f, z_{ref}\right)\right] \tag{4.5.5.3}$$

Where:

$$S_{cali}\left(f, z_{ref}\right) = \frac{4}{R(f)^2}\left|FT\left[RF_{cali}\left(t, z_{ref}\right)\right]\right|^2 \tag{4.5.5.4}$$

In eqn (4.5.5.3), the RF time signal of glass-water interface in depth $RF_{cali}\left(t, z_{ref}\right)$ is represented as $RF_{cali}\left(t, z_{ref}\right)$. And frequency-dependent pressure reflection coefficient of glass-water interface is represented as $R(f)$.

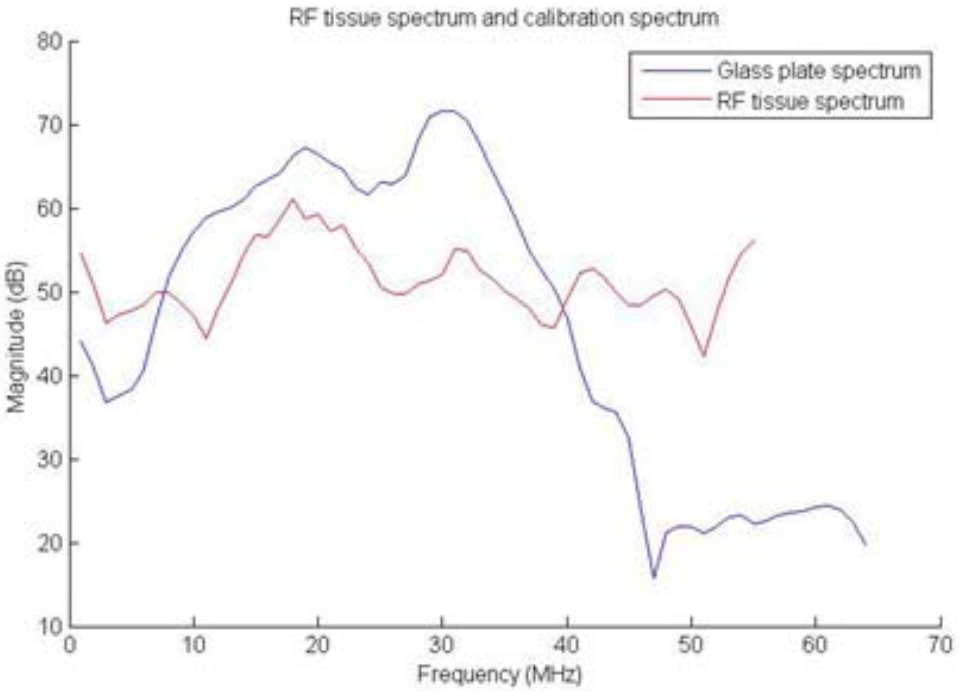

Figure 4.5 shows plot of RF tissue spectrum and glass plate spectrum. More unstable spectrum shape is observed in the uncalibrated RF spectrum. After calibration, the useful signal to noise ratio (SNR) region was expanded to 15－35MHz.

Linear regression was performed to the calibrated spectrum between 15－35MHz (Figure 4.6). The fit line is calculated to obtain slope (k), intercept with extension (I) and Amplitude (dB) in the center frequency (Midband fit M).

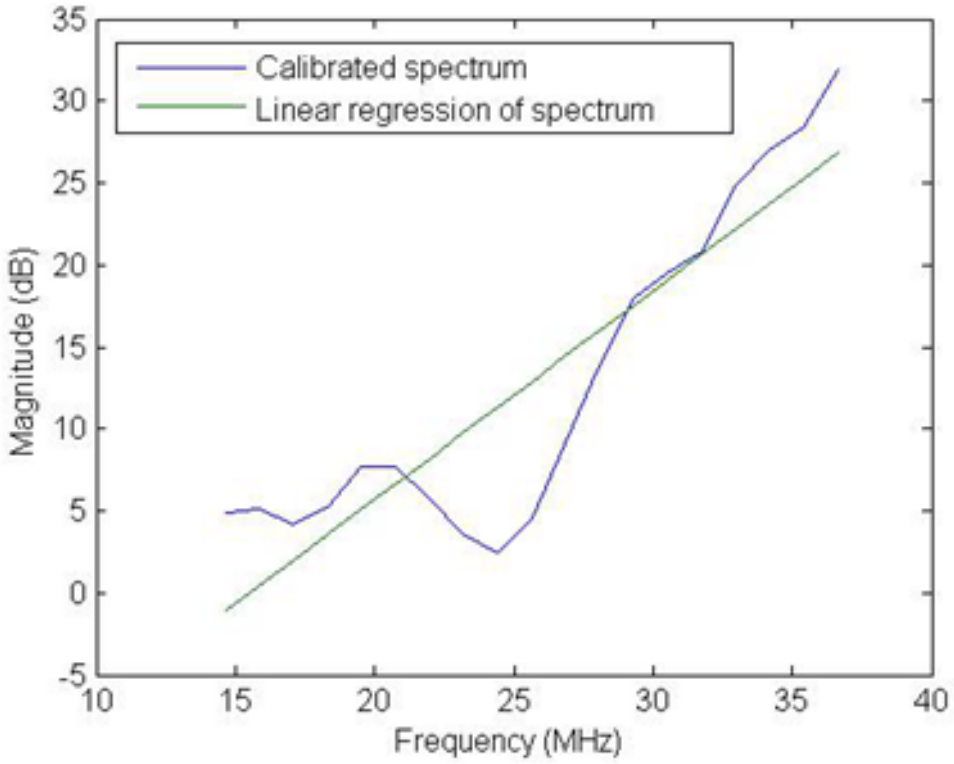

Figure 4.6. Linear regression was performed to the calibrated spectrum between 15—35MHz

For ultrasound echo above 30 MHz, the attenuation in the water could not be neglected. The relation between ideal parameter and practical parameter with attenuation compensation was discussed by other group (Lizzi et al., 1997):

$$I' = I \tag{4.5.5.5a}$$

$$k' = k - 2\alpha X \tag{4.5.5.5b}$$

$$M' = M - 2\alpha X f_c \tag{4.5.5.5c}$$

The ideal parameters without attenuation compensation are represented as I, k, M; while the practical parameters after attenuation compensation are represented as I', k' and M'.

The acoustic attenuation coefficient, the depth of ROI tissue and the center frequency are represented as α, X and f_c , respectively.

According to eqn (4.5.5.5), Intercept I (dB) is independent of attenuation, while slope k (dB/MHz) and midband fit M (dB) have linear relation with their ideal ones.

4.4.6 Parameter Statistical Analysis

The derived parameters (I, k and M) were divided into two groups—normal tissue group and cancer tissue group. Independent t-test was conducted between the two groups for statistical analysis. The assumption of t-test is that the two group data are natural distribution. Lizzi has proved that the probability density function (pdf) of k and I are Gaussian distributed in the histogram and M has Gaussian pdf feature when the analysis spectral cells more than 10 (Lizzi et al., 1997). In this work, I assume that k, I and M can be naturally distributed. The software used in this part was IBM SPSS Statistics (Version 20).

Because only two of the three parameters are functional independent, I assume that the combinations of two parameters could provide more tissue microstructural features than single alone. The statistical method of Fisher Linear Discriminant (FLD) was employed to explore the linear combination to distinguish the normal and cancer tissue. The

application assumption of FLD is that two compared groups are both natural distribution in probability density function. The equation of FLD is:

$$J_{fisher}(\varphi) = \frac{\varphi^T S_b \varphi}{\varphi^T S_w \varphi} \tag{4.5.6 .1}$$

Where, φ represents N dimension vector. The purpose of FLD is to obtain φ to maximize the value of $J_{fisher}(\varphi)$; then two under-test parameters are projected to the vector φ. The physical meaning of the equation is to find φ so that the two parameters which are projected to φ can have maximum value between-class scatter (S_b) and minimum within-class scatter (S_w). $S_b \; and \; S_w$ are expressed as:

$$S_b = \sum_{i=1}^{c} P(i)(u_i - u)(u_i - u)^T \tag{4.5.6 .2a}$$

$$S_w = \sum_{i=1}^{c} P(i)\, E\{(u_i - x)(u_i - x)^T | x \in class\ i\} \tag{4.5.6 .2b}$$

In eqn (4.5.6.2), u_i represents the mean value of class i; P(i) ($P(i) = \frac{n_i}{m}$) represents the probability of sample falling into class i.

$$W_{opt} = argmax \frac{|W^T S_b W|}{|W^T S_w W|} \quad (4.5.6\ .3)$$

The optimization function to obtain a projection matrix W_{opt} composed of a series of optimized discriminant vectors is represented in Eqn (4.5.6.3). W_{opt} is the eigenvector associated with the maximum eigenvalue in following eigenequation:

$$S_b \varphi_i = \lambda S_w \varphi \quad (4.5.6\ .4)$$

The calculated FLD value which relates to the three combinations of K, I and M was analyzed by independent t-test in SPSS between cancer group and normal tissue group again to test the significant difference.

4.4.7 Color Coded Image

Three FLD values were derived from three different combinations of k, I and M. Threshold was selected from the statistical analysis result to optimize the differentiation of the cancer tissue from normal tissue. Spectral parameter images display local values of FLD values of the combination of spectral slope, intercept and midband fit. Images are formed using a sliding hanning window (0.5mm) to progressively analyze RF data along each scan line. At each window region, averaged calibrated spectra (5 A-lines) are computed and corresponded to local values of spectral parameter. Every

combination of two parameters was projected to the FLD vector to compute the FLD values.

The FLD values were coded with the criteria form database. If the value falls into the cancer tissue band, the corresponding region would be coded in red; if normal tissue, it would be coded in green. Lastly, the parameter image was combined with original B-mode image. The color coded B-mode image could display complementary structural information and functional information.

4.5 EXPERIMENTAL RESULTS

4.5.1 Raw RF Data

A series of RF data was transformed to three dimension matrix vector (500 lines*2000 points*20 frames).

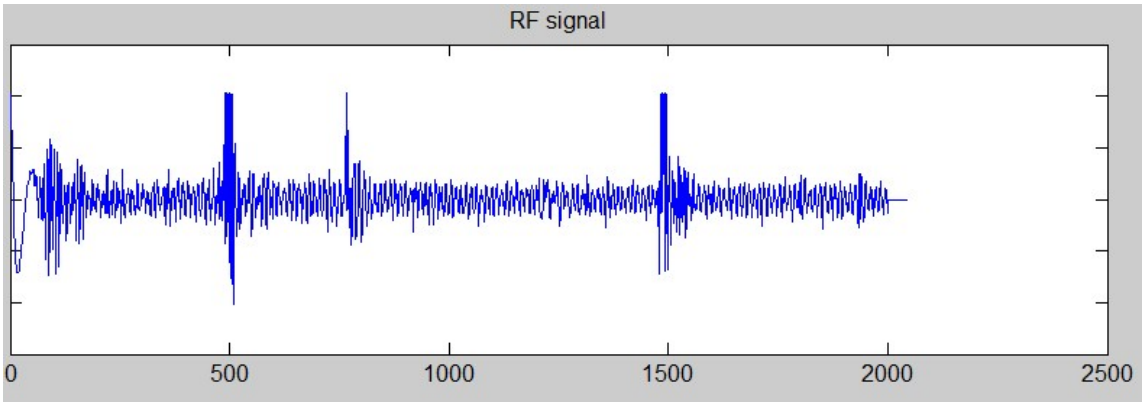

Figure 4.7. RF data of one scan line in time domain from *in vivo* normal rabbit colon tissue experiment

Figure 4.7 shows the typical RF data of one scan line in time domain from *in vivo* normal rabbit colon tissue experiment. The backscattered echo is clear enough to delineate. RF signal that the echo with relative large amplitude was backscattered by the interface with high acoustic impedance difference which may refer to the colon wall, water interface, transducer housing, position marker and air bubble.

4.5.2 B-Mode Image

Figure 4.8 shows B-mode image before and after band-pass filter (10MHz-65MHz, -9dB).

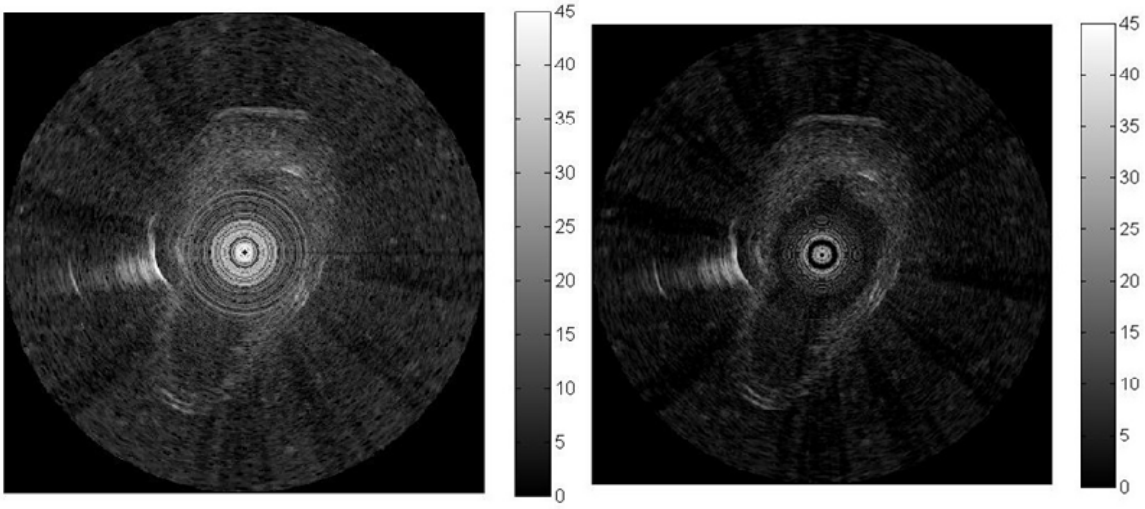

Figure 4.8. B-mode image before (left) and after (right) band-pass filter

In Figure 4.9, four typical value of dynamic range (35, 40, 45 and 50) can illustrate the way dynamic range influences the image quality and morphology information. In this part, the dynamic range was set to 45.

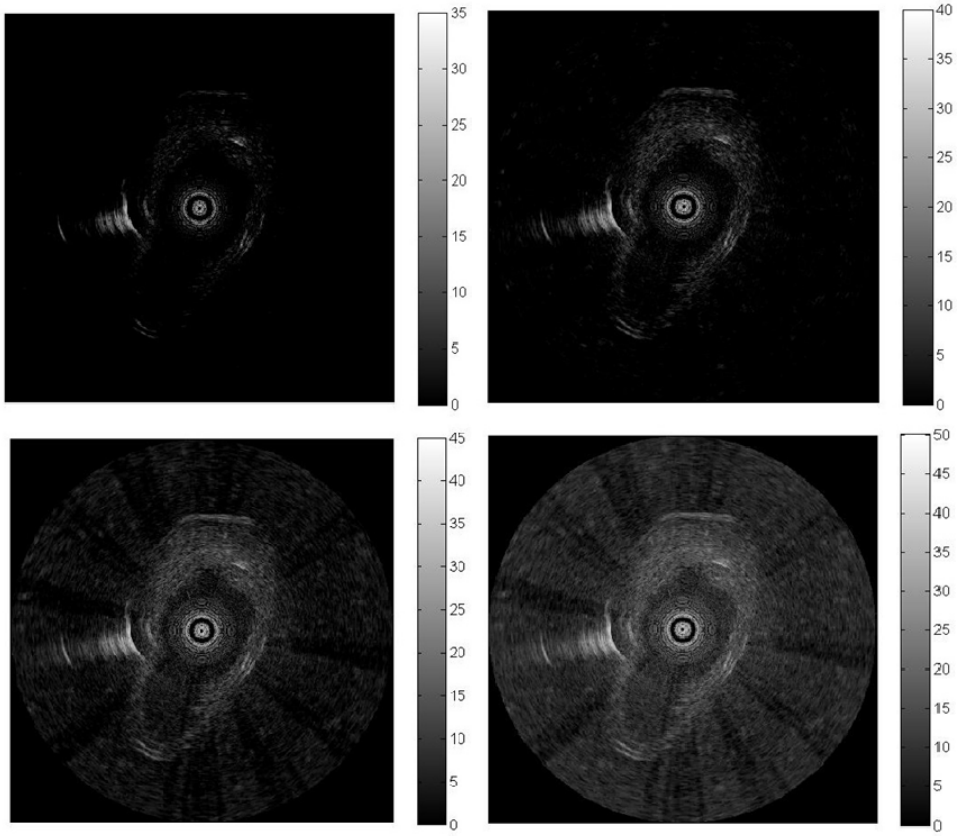

Figure 4.9 B-mode images in different Dynamic Range (upper left to right, 35dB, 40dB, lower left to right, 45dB, 50dB)

In Figure 4.10 several trials are made to find the optimal order of median filter in tradeoff between image quality and residual speckle noise. In this part, the order was set to 3.

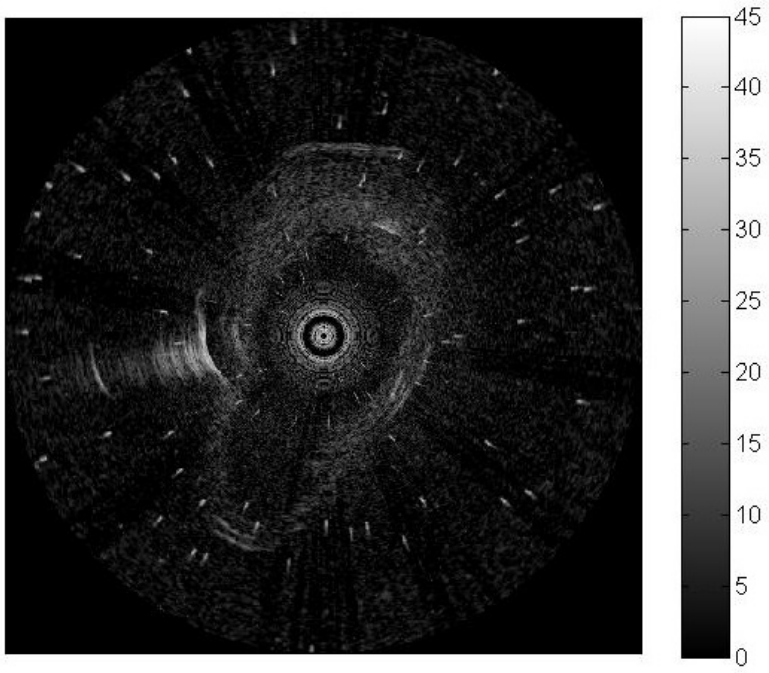

Figure 4.10 B-mode image without median filter

The final B-mode image is shown in Figure 4.11.

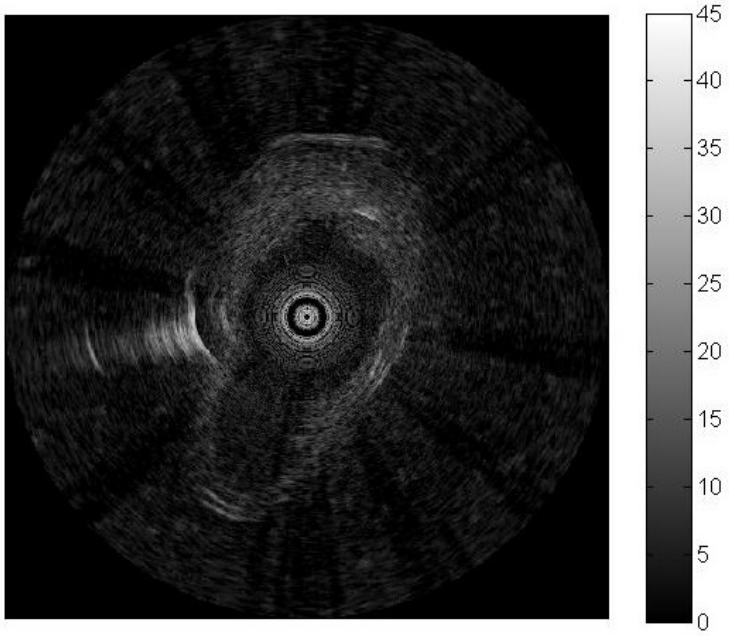

Figure 4.11 B-mode image with median filter

4.5.3 Parameter Statistical Test

Figure 4.12 shows the best fitting line calculated through linear regression test to the calibrated signal in the frequency range of 15-35MHz. Totally 90 samples (n=90) of ROIs were selected in normal tissue regions from 13 scan plane and 79 samples (n=79) of ROIs were selected in cancer tissue regions from 13 scan plane.

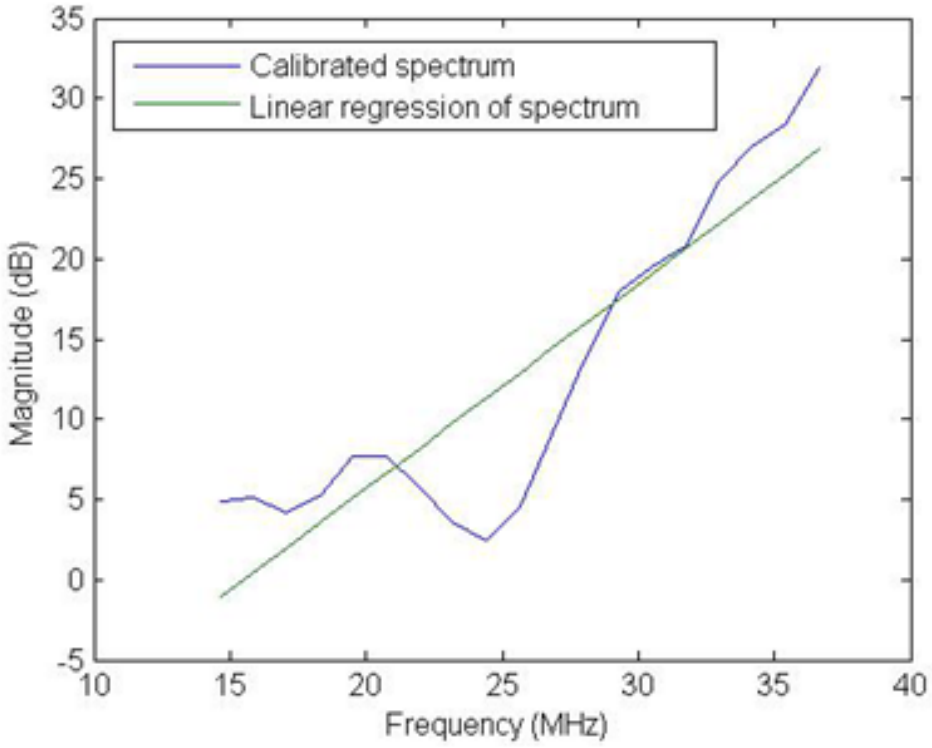

Figure 4.12 the best fitting line calculated through linear regression test to the calibrated signal in the frequency range of 15-35MHz.

After spectrum analysis, totally two groups (n=90 and n=79) including three parameter (k, I, M) in each group were ready for statistical test. The three parameters for two groups were described in means, standard deviation (SD) as shown in Table 4.1.

Table 4.1. The mean parameter values (k, I and M) of 90 normal tissue group and 79 cancer tissues group

Tissue Type	Mean value ± SD		
	Slope k (dB/MHz)	Intercept I (dB)	Midband Fit M (dB)
Normal tissue (n=90)	0.2857±0.2279	-20.9525±7.6356	-13.7966±3.7113
Cancer tissue (n=79)	0.2342±0.3368	-25.3867±10.6543	-19.7522±3.3587
Significant difference(*)	p=0.334	p=0.024*	p<0.001*

Significant difference between cancer tissue and normal tissue were observed for parameter I (p=0.024) and M (p<0.001), while no significant difference (p=0.334) was observed for the parameter k.

Figure 4.13 shows the normal distribution of I and M between normal tissue and cancer tissue. From the comparison of normal distribution, the boundary value is hard to delineate, thus if I or M were used as classifier for tissue type, the result would not be sensitive and specific enough.

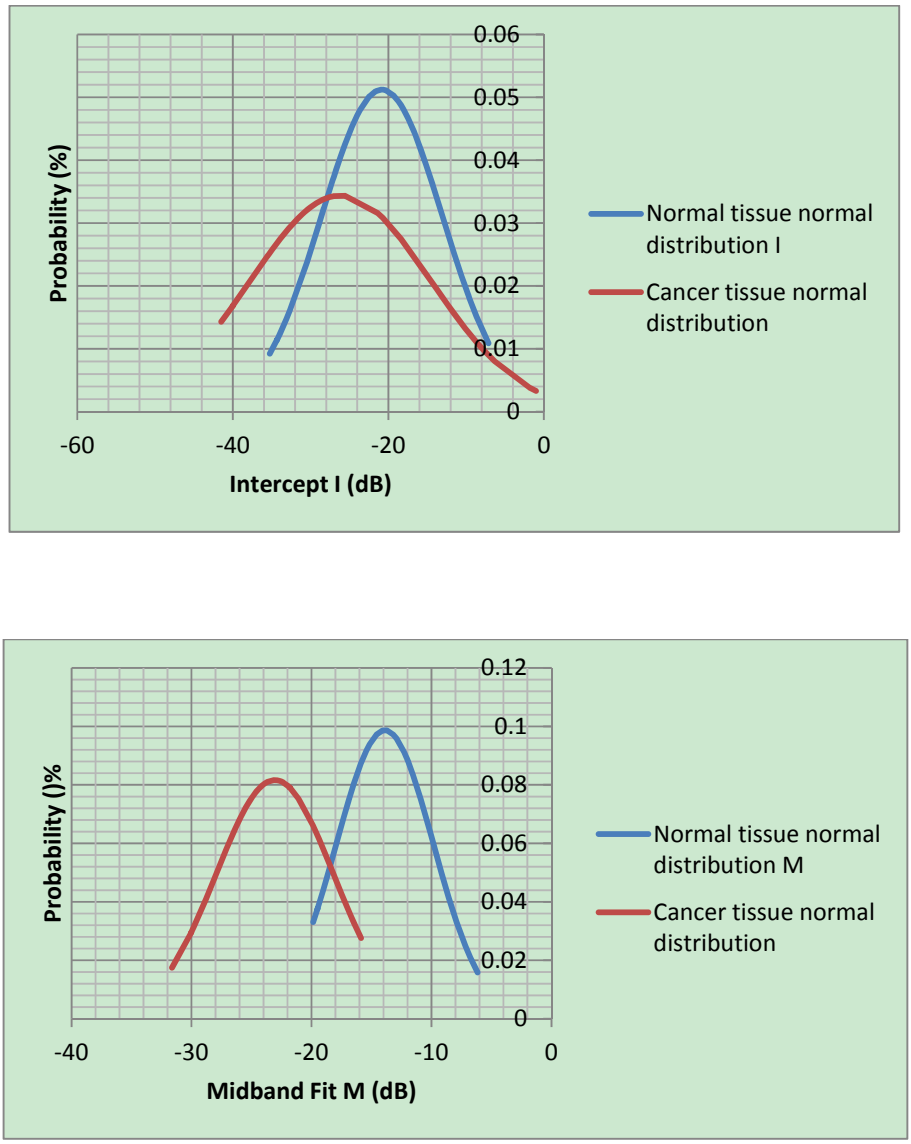

Figure 4.13 Normal distribution of I (upper) and M (below) between normal tissue and cancer tissue

Because two parameters from three are independent, the combinations of two parameters were expected to provide some information of tissue characterization. Figure 4.14 shows the plots of k with I.

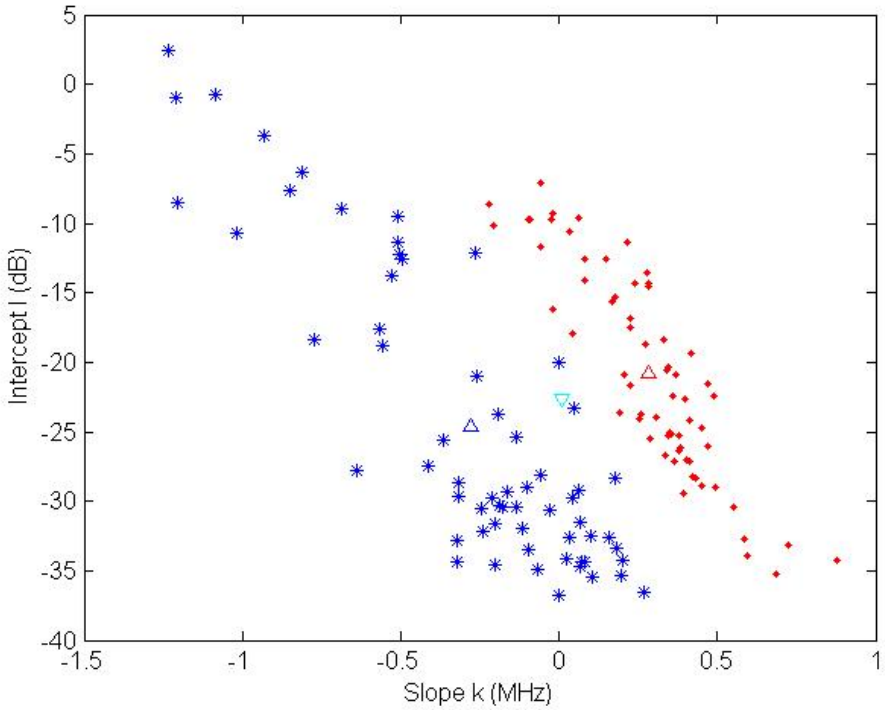

Figure 4.14 Plot of I and k; red represent normal tissue; blue represent cancer tissue; triangle is mean value

From the kI plot, the cancer tissue and normal tissue have a relative clear boundary. Further statistical analysis was done to the combinations of each two parameters after FLD process. The FLD value related to kI, kM and IM combination is described in Table 4-2 regarding mean value and standard deviation.

Table 4.2. The mean FLD values of each two parameter combination (k, I and M) of 90 normal tissue group and 79 cancer tissues group

Tissue Type	Mean value ± SD		
	FLD value of kI	FLD value of kM	FLD value of IM
Normal tissue (n=90)	0.3826±0.1184	1.4828±0.4818	8.7329±2.7244
Cancer tissue (n=79)	0.5467±0.0752	2.3059±0.3527	12.9261±1.9431
Significant difference(*)	$p<0.001$*	$p<0.001$*	$p<0.001$*

All of these three combinations show significant difference ($p<0.001$). Because two of the original parameters are independent, the combination of two parameters after FLD will have the same variance (between class variance and within class variance).

Thus the normal distribution of the three combinations was the same. Normal distribution of kI FLD value between cancer tissue and normal tissue as shown in Figure 4.15 are plotted to evaluate the predictability as classifier.

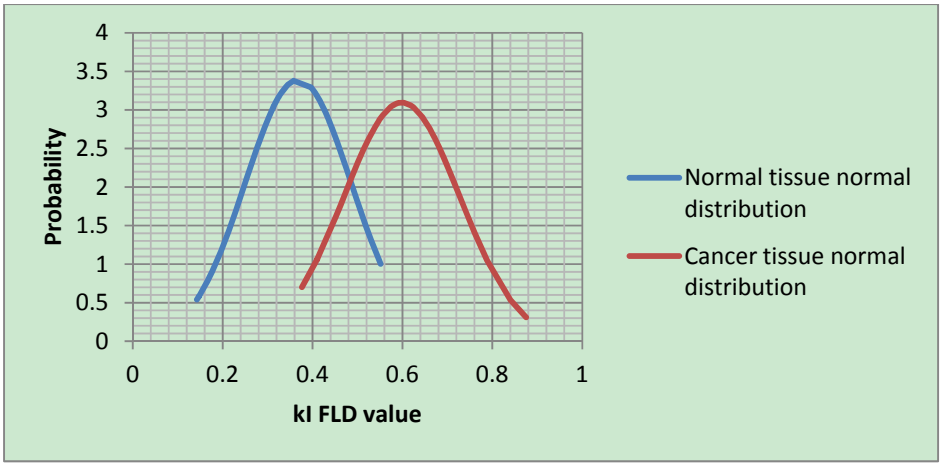

Figure 4.15 Normal distribution of FLD value of kI combination

kI FLD value was finally selected as the classifier to distinguish cancer tissue from normal tissue.

4.5.4 Color Coded Image

kI value was used to classify the tissue between cancer and normal tissue. The threshold was set to be 4.8; if the value in parameter image is larger than 4.8, the corresponded region is coded as red color; if less than 4.8, green color was coded. Thus red color region indicates the suspicious cancer tissue and green color indicates the water or normal tissue in Figure 4.16.

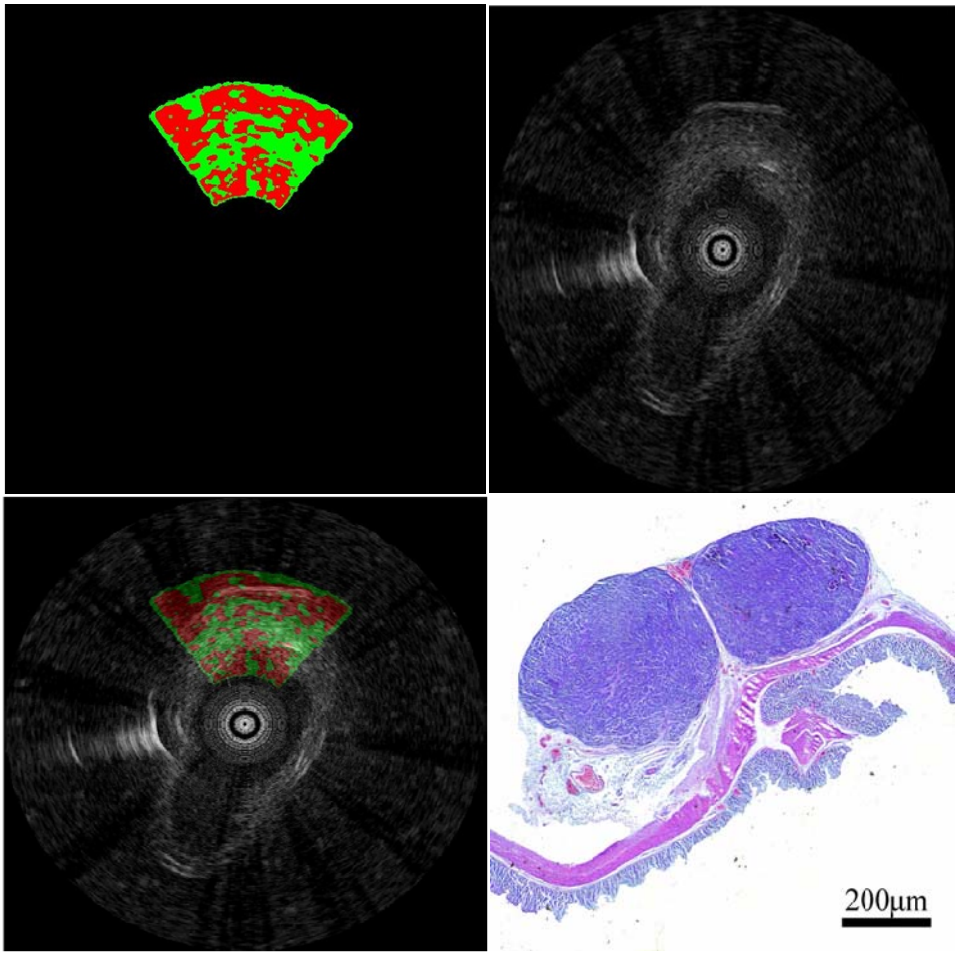

Figure 4.16 Upper left to right are color image and B mode image; Lower left to right are color coded image and histology result; red color represent cancer tissue; green color represents water or normal tissue

Each frame of image with colorectal tumor was determined by the inhomogeneous features along with adjacent homogeneous morphology of the colorectal wall. The histological specimen slices were obtained from a segment of colon tissue with tumor. B-mode image, color-coded image and histological image were visually compared and the pair which showed best match around the tumor region was shown in Figure 4.16. Nevertheless, perfect match among B-mode image, color-coded image and

corresponding histological image was impossible to be achieved because tissue detachments during microtome cutting would cause morphological alternations in the histological specimen.

4.6 DISCUSSION

In this chapter, frequency-domain analysis of the radio-frequency signals from a novel high-frequency endoscopic ultrasound system was performed to generate quantitative parameters for tissue characterization based on a rabbit model of colorectal cancer. To account for the response of the imaging system, the ultrasound spectra were calibrated by dividing the ultrasound spectra (radio-frequency ultrasound spectra from tissue) by the ultrasound spectrum from a perfect reflector excited under the same conditions. The resulting quasi-liner ultrasound spectra were fit by linear regression and midband fit, slope and intercept were computed from the best-fit line. These ultrasound spectral parameters were compared between the region-of-interests (ROIs) representing colorectal malignant tumors and adjacent normal colorectal wall tissue in a rabbit model. The mean midband fit and intercept in the ROIs showed significant differences between cancerous and noncancerous regions. These initial results suggest that such frequency-domain analysis can provide a quantitative method for tumor tissue characterization using EUS imaging. Statistical analysis showed that significant differences were observable between groups for mean FLD values of each two parameter combination (k, I and M) (*t* test, $P < .05$). The color coded image visually correlates with the histology result. It does not only depict morphological changes, but also could show functional

changes. When cancer is under progression, the first change is probably in cellular level which is not easy to detect in clinic, while the structural changes come much later along with the functional changes. The color-coded image along with histological result showed the potential of this method by measuring the function information and morphology information together for better diagnosis of early colorectal cancer in the future.

CHAPTER 5 CONCLUSIONS AND DISCUSSION

5.1 CONCLUSIONS

The first part of my work aimed to establish a novel high-frequency EUS system, which is able to provide enough precise structure image and compatible with other potential functional imaging tools, to delineate the depth- view structure of colorectal tract where an early abnormalities originates and to combine functional information for in vivo real-time patho-physiological histology. Outcome from this work demonstrated the potential of high-frequency EUS combining QUS technology for complementary high-resolution structural and patho-physiological diagnosis. The phantom experiment result and normal animal tissue experiment demonstrated the performance of the novel high-frequency EUS system; Figure 3.7 and Figure 3.8 depicted the layered colorectal tract structure of normal ICR mouse and New Zealand Rabbit by high-frequency EUS and the corresponding histology. The center of the lumen is occupied by the high-frequency EUS probe, represented by a gray circle that is surrounded by a bright area corresponding to the ultrasonic pulses multi-reflected between the transducer and the catheter wall. The innermost hyper-echoic circular layer is the mucosa (almost no lymphatic vessel), followed by the second hypo-echoic layer corresponding to the muscularis mucosa (lymphatic vessels appear on superficial surface). The third hyper-echoic layer is the submucosa (vascular and lymphatic vessels appear). The high-frequency EUS is able to delineate 30 μm differences of the layers in longitudinal direction.

The second part of my work was to perform frequency-domain analysis of the radio-frequency signals from the novel high-frequency endoscopic ultrasound system to generate quantitative parameters for tissue characterization. To account for the response of the imaging system, the ultrasound spectra were calibrated by dividing the ultrasound spectra (radio-frequency ultrasound spectra from tissue) by the ultrasound spectrum from a perfect reflector excited under the same conditions. The resulting quasi-liner ultrasound spectra were fit by linear regression and midband fit, slope and intercept were computed from the best-fit line. These ultrasound spectral parameters were compared between the region-of-interests (ROIs) representing colorectal malignant tumors and adjacent normal colorectal wall tissue in a rabbit model. The mean midband fit and intercept in the ROIs showed significant differences between cancerous and noncancerous regions. These initial results suggested that such frequency-domain analysis can provide a quantitative method for tumor tissue characterization. Statistical analysis showed that significant differences were observable between groups for mean FLD values of each two parameter combination (k, I and M) (*t* test, $P < .05$). Color-coded image along with histological result demonstrated the potential of this method for the diagnosis of colorectal cancer in the future.

5.2 DISCUSSION

The open strategy and programmable ability of the novel high-frequency EUS system make it suitable to implement the routine colonoscopy and other potential functional tools. The imaging characteristics such as frequency spectrum of the transmitted pulse,

parameter of the receiver filter, sampling rate, number of scan line, and length of scan line can be configured easily. The raw RF data can also be transferred and stored by the system. Multiple novel image processing algorithms such as tissue characterization based on ultrasound raw RF data and penetration improvement based on modulated excitation could be implemented on this customized system. The experiments on animal model of colorectal cancer (CRC) showed that mean FLD values of each two parameter combination of the backscattered signals obtained by using novel high-frequency EUS system can provide a noninvasive method to quantitatively discriminate between CRC and benign colorectal wall tissues. Multi-modality imaging combining high-frequency EUS and other functional tools, e.g. Photoacoustic (PAI), are rather potential in the field of colorectal cancer diagnosis.

As to the limitations of the work, firstly, 6 experimental rabbits were included in this experiment, but only 2 pieces of colon tissue samples with VX2 tumors were feasible for the ex vivo scan. Though totally 90 ROIs of normal tissue and 79 ROIs of cancer tissue were selected from 13 different scan planes, the sample volume is still not big enough. Secondly, the animal model of VX2 colorectal cancer is another limitation. The inoculation position is located at the outmost layer of rabbit colon due to the operation difficulty of transrectal operation. In clinic, most early stage cancer begins from the innermost layer of colon. The tumor development condition is also unknown.

In the future, the number of experiment subjects should be increased. Larger sample size would be useful and more reliable in evaluating the sensitivity and specificity of this method. Further experiments could employ *ex vivo* human colon tissue to test the

potential to apply this method in practical field. Before applying the method in clinical application, it is necessary to improve the fabrication and design of the endoscopic transducer for *in vivo* human RF data acquisition. Although the inherent compatibility of the system makes it suitable for complementing the routine endoscopy exam, the potential challenges for clinical applications still exist, such as differentiating different sub-type dysplasias and individual variances. Secondly, multi-modality imaging combining high-frequency EUS and other functional tools, e.g. Photoacoustic (PAI), are rather potential in the field of colorectal cancer diagnosis. Further studies may combine other functional imaging modalities with this novel EUS system to better facilitate the clinical strategy of colorectal cancer diagnosis.

REFERENCES

Alves KZ, Soletti RC, de Britto MA, de Matos DG, Soldan M, Borges HL, Machado JC. In Vivo Endoluminal Ultrasound Biomicroscopic Imaging in a Mouse Model of Colorectal Cancer. Acad Radiol 2012.

Anderson JC. Risk Factors and Screening for Colorectal Cancer. Colorectal Cancer Screening: Springer, 2011:7-23.

Atlanta: American Cancer Society. American Cancer Society. Colorectal Cancer Facts & Figures 2011-2013 2011.

Cannata JM, Ritter TA, Chen W, Silverman RH, Shung KK. Design of efficient, broadband single-element (20-80 MHz) ultrasonic transducers for medical imaging applications. Ultrasonics, Ferroelectrics and Frequency Control, IEEE Transactions on 2003;50:1548-57.

Chun, H., Cho, Y. And Lee, Y. Rectal Cancer: Preoperative Staging Using Endorectal Ultrasonography (Methodology). In: M.A. Hayat, Ed, Springer Netherlands, 2009; 317-327.

Copel, L., Sosna, J., Kruskal, J.B., Raptopoulos, V., Farrell, R.J. And Morrin, M.M., . Ct Colonography In 546 Patients With Incomplete Colonoscopy. Radiology, 2007; 244(2), 471-478.

Cornish, J.A., Tilney, H.S., Heriot, A.G., Lavery, I.C., Fazio, V.W. And Tekkis, P.P.,. A Meta-Analysis Of Quality Of Life For Abdominoperineal Excision Of Rectum Versus Anterior Resection For Rectal Cancer. Annals Of Surgical Oncology, 2007;14(7), Pp. 2056-2068.

Das A, Sivak Jr MV, Chak A, Wong RC, Westphal V, Rollins AM, Willis J, Isenberg G, Izatt JA. High-resolution endoscopic imaging of the GI tract: a comparative study of optical coherence tomography versus high-frequency catheter probe EUS. Gastrointest Endosc 2001;54:219-24.

Duda RO, Hart FE, Stork 0G. Pattern Classification. Canada: John Wiley & Sons, 2004.

Esteves FP, Schuster DM, Halkar RK. Gastrointestinal tract malignancies and positron emission tomography: an overview. Seminars in nuclear medicine, 2006:169.

E. Filoux, J. Mamou, O. Aristizabal, and J. A. Ketterling, Characterization of the spatial resolution of different high-frequency imaging systems using a novel anechoic-sphere phantom, IEEE Trans. Ultrason. Ferroelectr. Freq. Control, 2011; vol. 58, no. 5, pp. 994–1005.

Ferlay J, Shin H, Bray F, Forman, D, Mathers, C, Parkin D. GLOBOCAN 2008 v2.0, Cancer Incidence and Mortality Worldwide: IARC CancerBase No. 10 [Internet]. Lyon, France: International Agency for Research on Cancer 2010; Available from: http://globocan.iarc.fr, accessed on 20/5/2013.

Fayad, N. And Imperiale, T.. Noninvasive Screening Tests. In: M. Anderson Joseph And M. Kahi Charles, Eds, Humana Press, 2011; 123-150.

Flecknell P. Anaesthesia and analgesia for rodents and rabbits. Handbook of Rodent and Rabbit Medicine, Laber-Laird K, Swindle MM and Flecknell PA, eds., Pergammon Press, Butterworth-Heineman, Newton, MA 1996:219-37.

Gourtsoyiannis NC, Papanikolaou N, Karantanas A. Magnetic resonance imaging evaluation of small intestinal Crohn's disease. Best Practice & Research Clinical Gastroenterology 2006;20:137-56.

Hong Kong Cancer Stat 2007, Hong Kong Cancer Registry,Hospital Authority, 2009.

Haji A, Ryan S, Bjarnason I, Donaldson N, Papagrigoriadis S. Colonoscopic high frequency mini-probe ultrasound is more accurate than conventional computed tomography in the local staging of colonic cancer. Colorectal Disease 2012;14:953-9.

Huang CC, Sun L, Dailey SH, Wang SH, Shung KK. High frequency ultrasonic characterization of human vocal fold tissue. Journal of Acoustical Society of America. 2007;122: 1827-1832.

Huang CC, Ameri H, DeBoer C, Rowley AP, Xu X, Sun L, Humayun MS, Shung KK. Evaluation of the hardness of the lens in cataract surgery using high-frequency ultrasonic parameter in vitro. Ultrasound in Medicine and Biology. 2007;33:1609-1616.

Huang CC, Zhou Q, Ameri H, Wu D, Sun L, Humayun MS, Shung KK. Determining the acoustic properties of the lens using a high-frequency ultrasound needle transducer. Ultrasound in Medicine and Biology. 2007; 33:1971-1977.

Hurlstone DP, Sanders DS, Lobo AJ, McAlindon ME, Cross SS. Prospective evaluation of high-frequency mini-probe ultrasound colonoscopic imaging in ulcerative colitis: a valid tool for predicting clinical severity. Eur J Gastroenterol Hepatol 2005a;17:1325-31.

Hurlstone DP, Brown S, Cross SS, Shorthouse AJ, Sanders DS. High magnification chromoscopic colonoscopy or high frequency 20 MHz mini probe endoscopic ultrasound staging for early colorectal neoplasia: a comparative prospective analysis. Gut 2005b;54:1585-9.

Hurlstone P, Brown S, Baraza W. Endoscopic Resection of Early Colorectal Tumors: Novel Diagnostic and Therapeutic Techniques. Colorectal Cancer: Springer, 2009:155-69.

Jemal A, Siegel R, Xu J, Ward E. Cancer statistics, 2010. CA Cancer J Clin. Sep-Oct 2010; 60(5):277-300.

Joseph H. Sellin, Hector Oyarzabal, and Edward J. Cragoe，Electrogenic Sodium Absorption in Rabbit Cecum In Vitro，J. Clin. Invest. Volume 81, April 1988, 1275-1283

Kalisz, A.. Original Contribution Statistical Framework For Ultrasonic Spectral. Ultrasound In Medicine Biology, 1997; 13(9). 1371-1371-1382.

Kelly S, Harris K, Berry E, Hutton J, Roderick P, Cullingworth J, Gathercole L, Smith M. A systematic review of the staging performance of endoscopic ultrasound in gastro-oesophageal carcinoma. Gut 2001;49:534-9.

Kim SH, Lee JM, Eun HW, Lee MW, Han JK, Lee JY, Choi BI. Two-versus Three-dimensional Colon Evaluation with Recently Developed Virtual Dissection Software for CT Colonography1. Radiology 2007;244:852-64.

Kobaek-Larsen M, Thorup I, Diederichsen A, Fenger C, Hoitinga MR. Review of colorectal cancer and its metastases in rodent models: comparative aspects with those in humans. Comp Med 2000;50:16-26.

Kumon RE, Repaka A, Atkinson M, Faulx AL, Wong RC, Isenberg GA, Hsiao Y, Gudur MS, Deng CX, Chak A. Characterization of the pancreas in vivo using EUS spectrum analysis with electronic array echoendoscopes. Gastrointest Endosc 2012.

Lightdale CJ, Kulkarni KG. Role of endoscopic ultrasonography in the staging and follow-up of esophageal cancer. Journal of clinical oncology 2005;23:4483-9.

Lizzi, Frederic L Ostromogilsky, Michael Feleppa, Ernest J Rorke, Mary C Yaremko, Mykola M. Relationship Of Ultrasonic Spectral Parameters To Features Of Tissue Microstructure, Ieee Transactions On Ultrasonics. Ferroelectrics, And Frequency Control, 1986: 319-319-329.

Lizzi Fl, Feleppa Ej, Alam Sk, Deng Cx. Ultrasonic Spectrum Analysis For Tissue Evaluation. Special Issue On Ultrasonic Image Processing And Analysis. Pattern Recog Lett 2003;24:637–658.

Madsen EL, Frank GR, McCormick MM, Deaner ME, Stiles TA. Anechoic sphere phantoms for estimating 3-D resolution of very-high-frequency ultrasound scanners. Ultrasonics, Ferroelectrics and Frequency Control, IEEE Transactions on 2010;57:2284-92.

Matsumoto T, Hizawa K, Esaki M, Kurahara K, Mizuno M, Hirakawa K, Yao T, Iida M. Comparison of EUS and magnifying colonoscopy for assessment of small colorectal cancers. Gastrointest Endosc 2002;56:354-60.

Messina CR. Barriers to Colorectal Cancer Screening: Patient, Physician, and System Factors. Colorectal Cancer Screening: Springer, 2011:57-66.

Menzel, J. And Domschke, W. Gastrointestinal Miniprobe Sonography: The Current Status. The American Journal Of Gastroenterology, 2000; 95(3): 605-616.

Miller LS, Liu JB, Klenn PJ, Dhuria M, Feld RI, Goldberg BB. High-frequency endoluminal ultrasonography of the esophagus in human autopsy specimens. J Ultrasound Med. 1993;12:563–566

Osborn, N.K. And Ahlquist, D.A.. Stool Screening For Colorectal Cancer: Molecular Approaches. Gastroenterology, 2005; 128(1): 192-206.

Pietra N, Sarli L, Costi R, et al.: Role of follow-up in management of local recurrences of colorectal cancer: a prospective, randomized study. Dis Colon Rectum 1998; 41 (9): 1127-33.

Qiu W, Chen Y, Li X, Yu Y, Cheng WF, Tsang FK, Zhou Q, Shung K, Dai J, Sun L. An open system for intravascular ultrasound imaging. Ultrasonics, Ferroelectrics and Frequency Control, IEEE Transactions on 2012a;59:2201-9.

Qiu W, Yu Y, Tsang FK, Sun L. An FPGA-based open platform for ultrasound biomicroscopy. Ultrasonics, Ferroelectrics and Frequency Control, IEEE Transactions on 2012c;59:1432-42.

Rockey, D.C., Paulson, E., Niedzwiecki, D., Davis, W., Bosworth, H.B., Sanders, L., Yee, J., Henderson, J., Hatten, P., Burdick, S., Sanyal, A., Rubin, D.T., Sterling, M., Akerkar, G., Bhutani, M.S., Binmoeller, K., Garvie, J., Bini, E.J., Mcquaid, K., Foster, W.L., Thompson, W.M., Dachman, A. And Halvorsen, R. Analysis Of Air Contrast Barium Enema, Computed Tomographic Colonography, And Colonoscopy: Prospective Comparison. Lancet, 2005; 365(9456): 305-311.

Secco GB, Fardelli R, Gianquinto D, et al.: Efficacy and cost of risk-adapted follow-up in patients after colorectal cancer surgery: a prospective, randomized and controlled trial. Eur J Surg Oncol 2002; 28 (4): 418-23.

Siegel R, Naishadham D, Jemal A. Cancer statistics, 2013. CA: A Cancer Journal for Clinicians 2013;63:11-30.

Smith AJ, Driman DK, Spithoff K, Hunter A, McLeod RS, Simunovic M, Langer B. Guideline for optimization of colorectal cancer surgery and pathology. J Surg Oncol 2010;101:5-12.

Sobin, L., Gospodarowicz, M. And Wittekind, C., Eds. Tnm Classification Of Malignant Tumours. 7th Edition Edn. London, Uk: Wiley-Blackwell, 2009.

Sun L, Lien C, Xu X, Shung KK. In Vivo Cardiac Imaging of Adult Zebrafish Using High Frequency Ultrasound (45-75 MHz). Ultrasound Med Biol 2008a;34:31-9.

Sun L, Richard WD, Cannata JM, Feng CC, Johnson JA, Yen JT, Shung KK. A high-frame rate high-frequency ultrasonic system for cardiac imaging in mice. Ultrasonics, Ferroelectrics and Frequency Control, IEEE Transactions on 2007;54:1648-55.

Sun L, Xu X, Richard WD, Feng C, Johnson JA, Shung KK. A High-Frame Rate Duplex Ultrasound Biomicroscopy for Small Animal Imaging. Biomedical Engineering, IEEE Transactions on 2008b;55:2039-49.

Sun Y, Park J, Stephens DN, Jo JA, Sun L, Cannata JM, Saroufeem RM, Shung KK, Marcu L. Development of a dual-modal tissue diagnostic system combining time-resolved fluorescence spectroscopy and ultrasonic backscatter microscopy. Rev Sci Instrum 2009;80:065104,065104-7.

Wang Y, Zhou C, Hao Y, Li L, Liu S, Feng X, Zhou Z, Leung VY. Improvement in T-Staging of Rectal Carcinoma: Using a Novel Endorectal Ultrasonography Technique with Sterile Coupling Gel Filling the Rectum. Ultrasound Med Biol 2012;38:574-9.

Waxman I, Saitoh Y, Raju GS, Watari J, Yokota K, Reeves AL, Kohgo Y. High-frequency probe EUS-assisted endoscopic mucosal resection: a therapeutic strategy for submucosal tumors of the GI tract. Gastrointest Endosc 2002;55:44-9.

Xin-Mei Liang, Guang-Yu Tang, Ying-Sheng Cheng, Bi Zhou，Evaluation of a rabbit rectal VX2 carcinoma model using computed tomography and magnetic resonance imaging, World J Gastroenterol 2009 May 7; 15(17): 2139-2144

X. Li, W. Wu, Y. Chung, Q. Zhou, K. K. Shung, 80-MHz intravascular ultrasound transducer using PMN-PT free-standing film, Ultrasonics, 2011; 58: 11:2281-2288.

Yang J, Favazza C, Chen R, Yao J, Cai X, Maslov K, Zhou Q, Shung KK, Wang LV. Simultaneous functional photoacoustic and ultrasonic endoscopy of internal organs in vivo. Nat Med 2012;18:1297-302.

Zhou Q, Xu X, Gottlieb E, Sun L, Cannata JM, Ameri H, Humayun MS, Han P, Shung S. PMN-PT single crystal, high-frequency ultrasonic needle transducers for pulsed-wave Doppler application. Ultrasonics, Ferroelectrics and Frequency Control, IEEE Transactions on 2007;54:668-75.

Zhu Q, Hegde PU, Ricci A, Kane M, Cronin EB, Ardeshirpour Y, Xu C, Aguirre A, Kurtzman SH, Deckers PJ. Early-Stage Invasive Breast Cancers: Potential Role of Optical Tomography with US Localization in Assisting Diagnosis1. Radiology 2010;256:367-78.